Functional specialization of the yeast Rho1 GTP exchange factors

Sue Ann Krause[1$], Michael J. Cundell[2$], Pak P. Poon[3], Josephine McGhie[1], Gerry C. Johnston[3], Clive Price[2] and Joseph V. Gray[1]*

[1] School of Life Sciences
College of Medical, Veterinary and Life Sciences
Rm. 218 Davidson Building
University of Glasgow
Glasgow G12 8QQ
United Kingdom

[2] School of Health and Medicine
Division of Biomedical and Life Sciences
Lancaster University
Lancaster LA1 4YQ
United Kingdom

[3] Department of Biochemistry and Molecular Biology
Dalhousie University
Halifax, Nova Scotia
Canada B3H 1X5

$ These authors contributed equally to this work.

* Author for correspondence (Joseph.Gray@glasgow.ac.uk)

Running title: The yeast Rho1 GEFs

Summary

Rho GTPases are regulated in complex spatiotemporal patterns that may be dependent, in part at least, on the multiplicity of their GTP exchange factors (GEFs). Here, we examine the extent of and basis for functional specialization of the Rom2 and Tus1 GEFs that activate the yeast Rho1 GTPase, the ortholog of mammalian RhoA. First, we find that these GEFs selectively activate different Rho1-effector branches. Second, the synthetic genetic networks around *ROM2* and *TUS1* confirm very different global *in vivo* roles for these GEFs. Third, the GEFs are not functionally interchangeable: Tus1 cannot replace the essential role of Rom2, even when overexpressed. Fourth, we find that Rom2 and Tus1 localize differently: Rom2 to the growing bud surface and to the bud neck at cytokinesis; Tus1 only to the bud neck but in a distinct pattern. Finally, we find that these GEFs are dependent on different protein co-factors: Rom2 function and localization is largely dependent on Ack1, a SEL1 domain containing protein; Tus1 function and localization is largely dependent on the Tus1-interacting protein Ypl066w (which we name Rgl1). We have revealed a surprising level of diversity among the Rho1 GEFs that contributes another level of complexity to the spatiotemporal control of Rho1.

Key words: RHO1, GTP exchange factor, Cytokinesis, ROM2, TUS1

Introduction

The RhoA family of GTPases control cell morphogenesis and cytoskeletal structure and dynamics. For example, RhoA is key to the establishment and function of the cytokinetic actin ring (CAR) that is required for proper cytokinesis at the end of mitosis in yeast and in mammalian cells (Takaki et al., 2008). RhoA is also a protooncogene, reinforcing the importance of proper cell structure to locomotion and metastasis (Sahai and Marshall, 2002; Struckhoff et al., 2011).

Rho GTPases, including RhoA, appear to function in very complex spatiotemporal patterns to drive proper cell morphogenesis (Pertz et al., 2006; Pertz, 2010). For example, recent work in mammalian cells points to RhoA being localized to discrete zones at the leading edge of a motile cell, as well as to distinct foci at the trailing edge of the cell (Pertz et al., 2006). This distribution at the cell cortex is highly dynamic and points to tight regulation of the position and activity of the GTPase as a function of time and movement. How such complex spatiotemporal patterns of RhoA activity are established is not well understood, but is likely to be dependent on spatiotemporal control of key regulators including the GTP exchange factors (GEFs) and GTPase activating proteins (GAPs) that directly affect its GTP status.

The role of GEFs in the fine control of Rho GTPases is suggested by a number of observations. The number of potential Rho GEFs in any eukaryote is significantly more than the number of characterized Rho GTPases, e.g., some 69 putative Rho GEFs are found in the human genome sequence compared with 22 Rho GTPases (Rossman et al., 2005; Garcia-Mata and Burridge, 2007). Thus, there is sufficient plurality in the GEF population to localize and activate Rho GTPases in very complex patterns. Indeed, some GEFs can alter the specificity of their target Rho GTPase. For example, the Tiam1 GEF can directly bind to the Rac effectors IRSp53 and Wave2 thereby selectively activating only these Rac effectors (Connolly et al., 2005).

The complexities of Rho GTPase signalling also apply in other eukaryotes, including the budding yeast *Saccharomyces cerevisiae*. The yeast RhoA ortholog, Rho1, appears to be regulated in a complex spatiotemporal pattern, acting at the growing bud surface during bud growth (Levin, 2005), at the bud neck during cytokinesis (Piekney et al., 2005;

Wolfe and Glotzer, 2009) and at the vacuolar membrane where it mediates vesicle fusion and activation of the ABC transporter Ycf1 (Logan et al., 2010; Paumi et al., 2007).

Rho1 is a key, essential hub protein in the Cell Wall Integrity (CWI) pathway in which activated Rho1-GTP binds directly to and activates multiple different downstream effectors including Protein Kinase C (Pkc1) which is required for cell integrity, the β-1,3-glucan synthases Fks1 and Gsc2 critical for cell wall synthesis and the Bni1 formin, a key modulator of actin assembly ((reviewed in Levin, 2005).

Rho1 can be activated by a number of different signals and inputs. For example, the state of the cell surface is sensed by a number of cell surface sensors especially Wsc1/Hcs77 and Mid2 (Levin, 2005). Rho1 is also activated by Cyclin Dependent protein Kinase (CDK) at the G1/S transition (Kono et al., 2008) and by Polo kinase at cytokinesis (Yoshida et al., 2006). Furthermore, Rho1 activity is dependent on TORC2 signalling (Ho et al., 2008), TORC1 signalling (Petkova et al., 2010) and phospholipid metabolism (Audhya and Emr, 2002).

In yeast, three GEFs activate Rho1: Rom1, Rom2 and Tus1. Rom1 and Rom2 are highly homologous proteins with Tus1 being more distantly related (Levin, 2005). The Rom1 and Rom2 proteins contain a GEF/Dbl and a putative PH domain in the middle of the protein, domains characteristic of Rho GEFs (Rossman et al., 2005). The Rom1 and Rom2 proteins also contain a putative DEP domain N-terminal to the Dbl domain and a Citron Homology (CNH) domain at the C-terminus. This CNH domain is of unknown function but may be a protein-protein interaction domain that binds to Rho1 itself (Taira et al., 2004). Tus1 also contains a Dbl, a robust PH domain and CNH domains in the same order as in the Roms, but lacks a DEP domain.

The three Rho1 GEFs function together to activate Rho1 in vivo. An otherwise inviable mutant lacking all three GEFs can be kept alive either by expressing a mutant version of Rho1 that exchanges nucleotides rapidly or by the absence of one of the Rho1 GTPase-activating proteins, Sac7 or Lrg1, that inactivate Rho1 (Yoshida et al., 2009).

Rom1 and Rom2 appear to be largely redundant, but with Rom2 being the major isozyme. Loss of Rom2 causes cell lysis at high temperature whereas loss of Rom1 has little phenotypic consequence. However, loss of both proteins is lethal, causing cell lysis

at all temperatures (Ozaki et al., 1996). Rom2 may also be partly redundant with Tus1. Although loss of Tus1 alone results in only subtle phenotypes (Hillenmeyer et al., 2008; Lesage et al., 2005; Schmelzle et al., 2002), loss of both Tus1 and Rom2 results in a strong temperature sensitive growth defect (Schmelzle et al., 2002; Krause et al., 2008).

The Rho1 GEFs can be regulated similarly, e.g., Tus1 is an established, and Rom2 a probable, target of polo kinase (Cdc5) at cytokinesis (Yoshida et al., 2006). However, the GEFs can also be regulated differently, e.g., Tus1 is the only one of the three to be a substrate for cyclin-dependent protein kinase at the G1/S transition (Kono et al., 2008).

The GEFs themselves seem to localize in distinct patterns, but side-by-side comparison of the Rom proteins and Tus1 has not been made. Rom2 localizes to the growing bud surface and to the bud neck during cytokinesis (Manning et al., 1997; Kobayashi et al., 2005). Tus1 is found at the incipient bud site early in the cell cycle and at the bud neck at cytokinesis (Kono et al., 2008; Yoshida et al., 2006). The mechanisms of targeting the GEFs to their subcellular locations are not known save for the bud neck targeting of Tus1 and possibly Rom2 being triggered by phosphorylation by polo kinase Cdc5 (Wolfe and Glotzer, 2009; Yoshida et al., 2006).

The GEFs are critical for the proper localization of Rho1, but only at late anaphase. The targeting of Rho1 to the bud cortex during most of the cell cycle is dependent on actin polarization (Ayscough et al., 1999) but independent of the Rho1 GEFs (Yoshida et al., 2009). Indeed later, following actomyosin ring contraction, Rho1 accumulates at the bud neck via a GEF-independent mechanism that specifically requires the Rho1 PBS domain (Yoshida et al., 2009).

Here we mainly focus on the two major Rho1 GEFs, Rom2 and Tus1. We find that these GEFs selectively target different Rho1 effector pathways. We find that these GEFs play different *in vivo* roles, have distinct subcellular localization patterns and separate localization mechanisms dependent on different, novel proteins. Our observations point to a surprising level of functional specialization among the Rho1 GEFs.

Results

The Rho1 GEFs differentially affect different Rho1-effector pathways

Rho1 activates multiple different downstream effectors. It is possible that the Rho1 GEFs preferentially activate different subsets of effector pathways. We set out to determine the relative activity of three different effector branches in wild-type cells versus mutant cells lacking one of the Rho1 GEFs. In all cases, we failed to find any measurable consequence for the loss of Rom1, consistent with this isozyme playing a very minor role (data not shown). Here we focus on *rom2Δ* and *tus1Δ* mutants.

First, Rho1 activates the vacuolar transporter Ycf1, a member of the MDR family of transmembrane metabolite transporters. This transporter is required to accumulate a red metabolic end product in the vacuole of *ade2Δ* cells and the extent of accumulation of this red product is proportional to the *in vivo* transport activity of Ycf1 (Paumi et al., 2007). The accumulation of red pigment was assessed in double mutant *ade2Δ.rom2Δ* and *ade2Δ.tus1Δ* cells in comparison to *ade2Δ* single mutant cells. The absence of Tus1 severely compromised Ycf1 activity *in vivo*, whereas loss of Rom2 resulted in only a mild transport defect (**Fig. 1A**). Both GEFs clearly contribute to Rho1-Ycf1 activity, but Tus1 plays a more important role.

Second, Rho1 binds to and activates the plasma membrane glucan synthase enzyme that is required for the synthesis of β1,3-glucan (Levin, 2005). The steady state level of β1,3-glucan in the cell wall is dependent, at least in part, on Rho1 function. We assayed glucan levels in *rom2Δ* and *tus1Δ* mutant cells using the aniline blue glucan binding dye and assaying either total aniline blue staining of cell populations (Shedletzkey et al., 1997) or the fraction of buds that stain positively for the dye in small-budded cells (Sekiya-Kawasaki et al., 2002). We found that aniline blue staining was significantly reduced by loss of Rom2 but not by loss of Tus1 and in both assays (**Fig. 1B,C**). In contrast to the situation with Ycf1, our data are consistent with Rom2 playing a more important role than Tus1 in modulating the Rho1-glucan synthase effector pathway.

Third, Rho1 binds to and activates Pkc1, the yeast protein kinase C homolog. The activity of Rho1-dependent Pkc1 function can be monitored using an Rlm1-lacZ reporter construct whose expression reflects the *in vivo* activity of Rho1-Pkc1 signalling (Jung et

al., 2002). We measured the activity of this Rlm1-LacZ reporter in wild-type haploid and congenic deletion mutant cells grown in liquid cultures at room temperature. We found that mutant cells lacking Rom2 displayed reduced Rlm1-LacZ reporter activity, consistent with Rom2 serving as the main GEF controlling Rho1-Pkc1 (**Fig. 2A**).

Surprisingly, we found that mutant cells lacking the Tus1 GEF displayed *elevated* Rlm1-Pkc1 reporter activity (**Fig. 2A**), suggesting that Tus1 *inhibits* Rho1-Pkc1 activity. This high reporter activity faithfully co-segregated with the deletion mutation in genetic crosses with wild-type cells, indicating that it is not the consequence of secondary mutations (data not shown).

This high apparent activity of Rho1-Pkc1 signalling is also not an artefact of the assay system. Recent expression profiling identified 12 genes whose expression is strongly induced in a *tus1Δ* mutant (Benschop et al., 2010). We cross-referenced the expression of these genes in published profiles from cells in which Rho1-Pkc1 signalling is activated (Roberts et al., 2000). Of the 11 genes that are highly expressed in a *tus1Δ* mutant and for which data are available, 9 are induced when Pkc1 or Rho1 or both are activated in otherwise wild-type cells. Expression profiling is thus consistent with *high* activity of Rho1-Pkc1 signalling in the *tus1Δ* mutant.

If Tus1 is indeed an inhibitor of Rho1-Pkc1 activity, overexpression of the protein should lower activity of the pathway. To overexpress the Rho1 GEFs, *ROM2* and *TUS1* were placed under the control of the inducible *GAL1,10* promoter on a plasmid. We induced expression of the GEF genes in otherwise wild-type cells and assayed the consequence on Rlm1-LacZ reporter activity. We found that ectopic overexpression of *ROM2* resulted in elevated reporter activity, consistent with Rom2 activating Rho1 (**Fig. 2B**). In contrast, we found that ectopic overexpression of *TUS1* repressed reporter activity, consistent with its apparently paradoxical role as an inhibitor of Rho1-Pkc1 function (**Fig. 2B**).

Why is Pkc1 activity upregulated in *tus1Δ* cells? It is possible that loss of Tus1 may cause a defect in some Rho1-effector activity that is sensed by Rom-Rho1 complexes via a feedback loop resulting in activation of Pkc1 signalling. If this model is correct, then we expect the elevated activity of the Pkc1 branch in a *tus1Δ* mutant to be dependent on activation of one or both of the Roms. Triple mutant cells lacking all three GEFs are

inviable. We therefore assayed Rlm1-LacZ reporter activity in the double mutant cells lacking Tus1 and either Rom2 or Rom1. The *tus1Δ.rom1Δ* and *tus1Δ.rom2Δ* double mutant cells were viable, although the latter were slow growing and temperature sensitive (Schmelzle et al., 2002; Krause et al., 2008). We found that Rlm1-LacZ reporter activity was significantly reduced in both of the double mutant cells compared to *tus1Δ s*ingle mutant cells (**Fig. 2C**). The high reporter activity seen in *tus1Δ* mutants is not suppressed by osmotic stabilization, suggesting that the absence of Tus1 is not triggering a cell surface defect. These data are consistent with, but does not definitively prove that, Tus1 indirectly affecting the Rho1-Pkc1 effector branch by feedback control via both Rom1 and Rom2 (see Discussion). The Pkc1 effector pathway provides the most dramatic evidence for functional specialization of the Rho1-GEFs.

***ROM2* and *TUS1* synthetic genetic interaction networks.**

The apparent functional differences between Rom2 and Tus1 may be reflected in their global *in vivo* roles? The set of synthetic lethal or synthetic sick (SSL) genetic interactions for a gene gives an unbiased view of the global *in vivo* function of a query gene product. Here, we determined the networks of null-null SSL genetic interactions using *rom2Δ* or *tus1Δ* as query mutations and screened against the haploid deletion collection of ~4,700 single mutants using Synthetic Genetic Array (SGA) analysis (Tong et al., 2001; Tong et al., 2004). Putative SSL interactions, where double mutants were inviable or slow growing, were identified in triplicate screens and confirmed either by random spore analysis or tetrad dissection or both.

We found and confirmed 46 SSL interactions for *ROM2* (**supplementary material Table S1**) and 31 interactions for *TUS1* (**supplementary material Table S2**). Genes whose gene products act in cell organization and biogenesis or in transport dominate both of the networks. However, only five interactions are shared between the two networks (representing a mere 11% and 16% of each network respectively) (**Fig. 3A**). The SSL genetic networks are thus consistent with related but largely distinct *in vivo* roles for Rom2 and Tus1.

The distinctive roles for the two major RhoGEFs is reinforced by considering SSL interactions that occur between the GEF genes and genes encoding other known components of the Rho1 signalling pathway. *ROM2* interacts with *ROM1*, *MID2* and *ACK1*, genes encoding known upstream activators of Rho1-Pkc1 signalling; *BCK1*, *SLT2* and *SWI6*, genes encoding components of the Pkc1-MAP kinase pathway; and *FKS1*, the gene encoding a glucan synthase isozyme, another Rho1 effector (**Fig. 3B**). In contrast, *TUS1* interacts with *SPA2*, *PEA2* and *BNI1*, genes encoding components of the polarisome complex (**Fig. 3C**) and where Bni1 is another direct effector of Rho1. Only one gene *SWI6*, encoding a target of Rho1-Pkc1 signalling but with other independent functions, is found in both SSL networks.

Tus1 cannot replace the Roms

Loss of Rom2 results in a number of mutant phenotypes including hyper-sensitivity to benomyl treatment (Manning et al, 1997; our unpublished work). In contrast, loss of *TUS1* leads to distinct phenotypes including hypersensitivity to chlorpromazine (our unpublished work). Importantly, we found that overexpression of *TUS1* suppressed the hypersensitivity of *rom2Δ* mutant cells to benomyl and that overexpression of *ROM2* suppressed the hypersensitivity of *tus1Δ* mutant cells to chlorpromazine (**supplementary material Fig. S1A**). It thus appears that, under these conditions, overexpression of Rom2 can directly replace or compensate for the loss of *TUS1* and vice versa.

Can overexpression of *TUS1* suppress the inviability of *rom1Δ.rom2Δ* mutant cells lacking both Rom proteins? Over-expression of *TUS1* was achieved either using a high copy plasmid containing the *TUS1* gene and its normal regulatory elements (p*TUS1*) (Schmelzle et al., 2002) or a high copy plasmid in which expression of *TUS1* is under the control of the *GAL1,10* promoter (pGAL-*TUS1*) (Krause et al., 2008). These plasmids are sufficiently potent to suppress the lethality of *tor2* mutants (Schmelzle et al., 2002: our unpublished work) and should thus be potent enough to suppress the lethality of *rom1Δ rom2Δ* double mutants if capable of doing do. The viability of haploid *rom1Δ.rom2Δ* transformants was determined in two ways. First, haploid double mutant cells harbouring one of the *TUS1*-expressing plasmids were generated by tetrad dissection of transformed double mutant diploid cells that were heterozygous for the

rom1Δ and *rom2Δ* mutations. Viability of transformed double mutant haploid progeny was assessed on the appropriate media. Second, *rom1Δ.rom2Δ* haploid cells rendered viable by a *URA3*-marked plasmid containing the wild-type *ROM2* gene were transformed with one of the *TUS1*-expressing plasmids. The ability of the doubly transformed cells to lose the *URA3*-marked plasmid containing *ROM2* was assessed by growth in the presence of 5 fluoroorotic acid (5FOA) and on the appropriate media.

In each experiment, we found that overexpression of *TUS1* either via p*TUS1* or pGAL-*TUS1* could not suppress the inviability of cells lacking both *ROM1* and *ROM2* (**supplementary material Fig. S1B**; data not shown). These data suggest that Rom1 and Rom2 share a unique, essential role that cannot be performed by Tus1, even when overexpressed.

Rom2 and Tus1 localize differently

Are the unique roles of the Tus1 and Rom2 GEFs in part regulated through differential localizations? *TUS1* and *ROM2* were epitope-tagged with GFP at their endogenous locus in otherwise congenic wild-type haploid cells of the BY4741 strain background. These tagged alleles are functional, with the strains being phenotypically indistinguishable from untagged, wild-type strains (data not shown).

We only observed Tus1-GFP localization during mitosis/cytokinesis. Specifically, Tus1-GFP localised to the bud neck at late anaphase B where it formed a continuous ring that underwent a robust contraction event after spindle breakdown (**Fig. 4A** and **Supplementary material Fig. S2** and **Movie S1**). These observations indicate that Tus1 is an integral component of the cytokinetic actomyosin ring (CAR). Following CAR contraction, a second highly transient Tus1-GFP ring, with a weaker fluorescence signal intensity than the first, formed at the division site. This single Tus1-GFP ring then splits to form two rings of weak intensity on either side of the bud neck (**Fig. 4A** and **Supplementary material Fig. S2** and **Movie S1**). The transient single ring likely represents Tus1-GFP associated with rings on either side of the thin primary septum, but too close to be resolved by microscopy. Subsequent formation and growth of the secondary septum allows these two rings to be resolved, leading to the observed split ring

structures. Tus1-GFP was also observed at the division site following cell separation, typically on the daughter cell side **(Fig. 4A)**.

We found that Rom2-GFP localises differently to Tus1-GFP. Rom2-GFP appeared at very faint, often polarised cortical patch like structures throughout the cell cycle that were most obvious in timelapse movies (**Supplementary Movie S2**). However, at several points in the cell cycle, Rom2-GFP concentrated at distinct structures giving rise to robust non-patch like signals. Rom2-GFP was first observed to concentrate at the incipient bud site as a bright focus (**Fig. 5**). In small budded cells with a single spindle pole body, Rom2-GFP was highly polarised towards the bud cortex, but this cortical localization became more isotropic and patch like in medium to large budded cells with a short bipolar or anaphase spindle respectively.

In late anaphase, Rom2-GFP was lost from the bud cortex and repolarised towards the daughter cell side of the bud neck (Fig. 4B). Following spindle breakdown, in two dimensions (XY), Rom2-GFP appeared to localise as a continuous band at the division site (**Fig. 5**); however, reconstructions demonstrated that this band represents a discontinuous ring which in time-lapse movies did not appear to undergo a robust contraction event (**Supplementary material Fig. S3** and **Movie S2**). Instead, we occasionally observed what looked like Rom2-GFP passively tracking plasma membrane ingression (**Supplementary material Figs. S3B** and **S3C**). Thus, in contrast to Tus1-GFP, these data suggest that Rom2-GFP is not an integral component of the CAR.

Reminiscent of Tus1-GFP, Rom2-GFP then formed split rings of weak signal intensity on either side of the bud neck. Finally, prior to cell separation Rom2-GFP was often (but not always) lost from the mother cell side before that of the daughter, the latter signal typically persisting after cell separation (**Fig. 5**).

Ack1 functions with Rom2

We speculated that the different localization patterns and functions of Tus1 and Rom2 are due to different affinities for other, as yet unidentified partner proteins. Systematic analysis of the yeast proteome has identified a number of robust and novel protein-protein interaction modules (Benschop et al., 2010). Importantly, that analysis places

Rom2 and Tus1 in distinct complexes: Rom2 with the Ack1 protein, and Tus1 with the novel Ypl066w protein.

Ack1 is a SEL1-domain containing protein that we have encountered previously. First, we identified Ack1 as a novel protein of unknown function that is required, like Rom2, for normal basal activity of Rho1-Pkc1 (Krause et al., 2008). Indeed, overexpression of *ACK1*, like *ROM2*, stimulates Rho1-Pkc1 activity (Krause et al., 2008). Second, we found that *rom2Δ.ack1Δ* double mutants are inviable (see SSL networks above (**supplementary material Table S1**). This inviability, like that of *rom1Δ.rom2Δ*, could be alleviated by the loss of the Rho1 GAP, Lrg1, suggesting that Rho1 activity is also limiting in the *rom2Δ.ack1Δ* double mutant (data not shown). Thus Ack1, like Rom2, is an upstream activator of the Rho1-Pkc1 effector pathway. However, Ack1 must also act independently of Rom2 to promote Rho1 activity, possibly via Rom1.

Overexpression of Ack1 in otherwise wild-type cells stimulates Pkc1 signalling as reflected in elevated Rlm1-LacZ reporter activity (Krause et al., 2008). Interestingly, overexpression of Ack1 could not elevate Rlm1-LacZ activity in a *rom2Δ* mutant (**supplementary material Fig. S4A**) nor could it alleviate the growth defects of *rom1Δ.rom2Δ* or *rom2Δ.tus1Δ* double mutant cells (data not shown; Krause et al., 2008). Taken together, our data are consistent with Ack1 functioning with *both* Rom1 and Rom2, but predominantly with Rom2. However, the activity of the Rom proteins cannot be totally dependent on Ack1 since *ack1Δ* mutant cells are viable whereas *rom1Δ.rom2Δ* mutant cells are not.

Ypl066w functions with Tus1

Tus1 and Ypl066w proteins are found in the same complex (Benschop et al., 2010). Indeed, *tus1Δ* and y*pl066wΔ* mutant cells share very similar microarray expression profiles, consistent with a shared role (Benschop et al., 2010). Supporting this view, we found that *ypl066wΔ* mutants, like *tus1Δ* mutants, displayed high, rather than low, Rlm1-LacZ reporter activity, indicating elevated Rho1-Pkc1 pathway activity (**supplementary material Fig. S4B**). Moreover, double mutant cells lacking both *YPL066w* and *TUS1* were viable and did not display any synthetic phenotypes (**supplementary material**

Table S2). Furthermore, although overexpression of *TUS1* lowered Rlm1-LacZ activity in otherwise wild-type cells (see before), overexpression did not affect reporter activity in an *ypl066wΔ* mutant (**supplementary material Fig. S4B**). We conclude that Ypl066w functions with Tus1.

Localization of Rom2 is dependent on Ack1

We tested if the localization of Rom2 or Tus1 is altered in *ack1Δ* mutant cells. All localization of Rom2-GFP to the bud neck was completely lost in the absence of Ack1 (**Fig. 5B,C**). Additionally, a reduced proportion of *ack1Δ* cells with a single spindle pole body (typically small budded cells) successfully localised Rom2-GFP to the bud cortex (**Fig. 5E**), and, when it occurred, the signal intensity was dramatically (4.3 fold) weaker compared to wild type cells (**Fig. 5D**). Bud surface localization was also less persistent in the mutant and was already lost in cells with a short bipolar spindle (medium sized bud) (**Fig. 5E**). The localization of Rom2-GFP is thus profoundly dependent on Ack1.

In contrast, the localization of Tus1-GFP is unaffected by the absence of Ack1 (**supplementary material Fig. S5**). Ack1 is thus selectively required to localize Rom2 and not Tus1.

It is possible that the *ack1Δ* mutation affects Rom2-GFP localization indirectly by reducing the overall amount of the protein in the cell. However, we can rule this possibility out since the absence of Ack1 did not cause a decrease in the steady state level of Rom2-13myc or Tus1-13myc as assayed by Western blotting of whole cell protein extracts (**Fig. S7**). In conclusion, Ack1 behaves as a cofactor that is absolutely required to localize Rom2 (but not Tus1) to the bud neck at cytokinesis. The protein is also required for efficient localization of Rom2 to the bud cortex earlier in the cell cycle.

Localization of Tus1 is dependent on Ypl066w/Rgl1

We tested if the localization of Tus1 or Rom2 is altered in a *ypl066wΔ* mutant (**Fig. 4**). Tus1-GFP failed to localize efficiently to the bud neck at late anaphase (1% of anaphase *ypl066wΔ* cells (n=109) displayed a fluorescent signal at the bud neck, compared to 9%

(n=105) in wild type). Following spindle breakdown in the *ypl066wΔ* mutant, Tus1-GFP localised to the bud neck as a ring that underwent contraction (**Fig. 4B,C**), but the fluorescent signal intensity was drastically reduced (5.7 fold) in comparison to wild-type cells (**Fig. 4D**). Moreover, the second phase of ring localization is completely lost in the absence of Ypl066w (i.e., no split rings or signals at cell separation were detected – see **Fig. 4C**). This failure to detect a second wave of localization may indicate failure of this second phase in the mutant or it may be a consequence of reduced signal intensity, bringing the signal below our limit of detection.

Localization of Rom2-GFP was essentially normal in the *ypl066wΔ* mutant cells. There were subtle changes in the distribution of Rom2-GFP localisations at cytokinesis but these are likely to be secondary consequences of a subtle effect of the mutation on cytokinesis itself (**supplementary material Fig. S6**). Ypl066w thus appears to be selectively required for the proper localization of Tus1, but not Rom2.

We investigated whether the severe reduction in intensity of Tus1-GFP localization in the *ypl066wΔ* mutant may be due to a profound reduction in the steady state amount of the the protein. Western blot analysis of 13MYC-tagged alleles indicated that the steady state level of Tus1 (and indeed that of Rom2) was not affected by loss of Ypl066w (**supplementary material Fig. S7**). We conclude that Ypl066w is a cofactor that is required for the efficient localization of Tus1 during all phases of cytokinesis. This is the first known role for this novel gene product and we therefore name the gene RGL1 (**R**ho1 **G**EF **L**ocalizing).

Discussion

Here, we show that the two principal GEFs for the Rho1 GTPase, Rom2 and Tus1, function very differently: Tus1 cannot perform the essential function of Rom2 (**supplementary material Fig. S1A**) and the genetic interaction networks around *ROM2* and *TUS1* are largely distinct (**supplementary material Tables S1 and S2)**. Furthermore, we discovered some of the basis for these functional differences.

First, the Rho1 GEFs selectively activate different Rho1-effector branches (**Figs. 1, 2**). To our knowledge, this is the first reported evidence of effector specificity by yeast Rho GEFs. Surprisingly, we also found that Tus1 acts as an inhibitor of Rho1-Pkc1 signalling (**Fig. 2A,B**): an apparently paradoxical role for a Rho1 activator. A profound difference in effector specificity between Rom2 and Tus1 may resolve this paradox. If Tus1 and Rom2 activate distinct subsets of Rho1-effector complexes (as they appear to do), then loss of Tus1 might result in a cellular defect that triggers activation of Rho1-Pkc1 signalling by a signal communicated via the Rom GEFs. Loss of Tus1 could thus activate Rho1-Pkc1 activity. Indeed, Rho1 signalling is known to be under feedback control (reviewed in Levin, 2005) and lack of at least one Rho1 effector branch, Rho1-Bni1, is known to trigger activation of Rho1-Pkc1 activity (Krause et al., 2008). An alternative possibility is that loss of Tus1 simply liberates more Rho1 GTPase to be activated by the Rom GEFs. Such a model does not involve feedback control but is less parsimonious because loss of Tus1 should then lead to the activation of all Rho1 effector branches, and not just Rho1-Pkc1.

Our work provides the first evidence that the yeast Rho1 GEFs preferentially activate subsets of the available Rho1-effector complexes. The mechanism of this effector specificity remains to be clarified, but the yeast system might prove a good model for exploring this poorly understood and important aspect of GTPase function (Cherfils and Zeghouf, 2011).

How might the GEFs target different Rho1-effector complexes? One possible mechanism for effector specificity is co-localization, where a GEF and its cognate Rho1 effectors localize independently to the same subcellular compartment. Indeed, the distinct localization patterns of Rom2 and Tus1 (**Figs. 4, 5**) make this a tempting possibility.

However, this mechanism demands that the effectors localize independently of the GEFs, a condition that is not met in key cases. For example, the localizations of Pkc1 and Bni1 are dependent on, rather than independent of, activated Rho1 whose localization is in turn dependent on the GEFs (Andrews and Stark, 2000; Tolliday et al., 2002). Another possible mechanism for effector specificity involves effector tethering, where the GEF binds to both the GTPase and the effector to form a stable ternary complex, as appears to be the case for the Rac GEF Tiam1 and the Rac effectors IRSp53 and Wave2 in mammalian cells (Connolly et al., 2005). No physical association between a Rho1 GEF and any Rho1 effector has been reported to date. However, the association between Rom2 and Ack1 and between Tus1 and Ypl066w (Benschop et al., 2010) suggests that the GEFs are indeed part of novel, higher order complexes. It is possible that the GEFs associate with their cognate effectors on biological membranes but where the complexes do not survive routine biochemical purification. The search for such GEF complexes deserves renewed vigour.

Here, we also find that the sub-cellular localizations of Rom2 and Tus1 are different, complex and highly dynamic (**Figs. 4**, **5**). We found that Rom2, but not Tus1, localizes to the growing bud surface and to polarised cortical patches through the cell cycle. These observations are consistent with the key role that the Rom2 plays in proper growth of the bud surface, a function that Tus1 cannot perform.

Both Rom2 and Tus1 localize to the bud neck during cytokinesis, but in distinct patterns consistent with different primary roles: Rom2 in septum growth and Tus1 in CAR function. Rom2 localizes to the division site in late anaphase, but first to the daughter side of the bud neck and then, following spindle breakdown, to a discontinuous ring that does not undergo robust contraction (**Fig. 5**). We infer that Rom2-GFP does not associate with the CAR but tracks the base of the constricting plasma membrane either side of the forming primary septum. Rom2 then forms discontinuous rings on either side of the bud neck during formation of secondary septum. The ring on the mother cell side is preferentially (but not always) lost prior to cell separation, whilst the ring on the daughter cell side persists after cell separation. Together, these localisation patterns support a primary role for Rom2 in promoting septation, consistent with prior genetic analysis (Yoshida et al., 2006; Yoshida et al., 2009). In contrast to Rom2, Tus1 initially localizes

to a single ring at the bud neck in late anaphase (**Fig. 4**). This ring contracts to a single focus following spindle breakdown consistent with Tus1 being an integral component of the CAR, as was suggested by previous work (Yoshida et al., 2006, 2009). After CAR contraction, there is a second, weaker localization of Tus1 to a highly transient ring structure at the bud neck that subsequently appears to split into two rings..

It is already known that the Rho1 GEFs themselves are required for the specific localizations of Rho1 in all phases of the cell cycle up to CAR contraction (Yoshida et al., 2009). Our discovery of the complex and distinct localizations of Rom2 and Tus1 suggest that each GEF contributes to a distinct subset of this dynamic localization, and thus localized activation, of Rho1. Later in cytokinesis, after CAR contraction, Rho1 can be localized independently of the GEFs to the bud neck (Yoshida et al., 2009). However, the activity of Rho1 is still dependent on the GEFs at this late stage in cytokinesis (Yoshida et al. 2009). The zone of active Rho1 in late cytokinesis is thus dictated by the localizations of Rho1 and the GEFs (and presumably the GAPs, which may also be functionally diverse: Schmidt et al., 2002) and their intersection.

The dynamics of Rho1 GEF localization at cytokinesis is unexpectedly complex, a complexity that may be required to properly control and orchestrate the different phases of cytokinesis and cell separation. Indeed, our discovery of the effector selectivity of the GEFs allows for different Rho1-effector branches to be activated in complex spatiotemporal patterns during cytokinesis. For example, it is tempting to speculate that, during cytokinesis, Tus1 selectively localizes and activates Rho1-Bni1 to drive CAR formation, whereas Rom2 primarily localizes and activates Rho1-Pkc1 to drive membrane and cell wall synthesis during septation. Much work remains to be done to test this model.

Here, we also report specific molecular roles for two novel regulators of Rho1 signalling, Ack1 and Rgl1(Ypl066w) (**Figs. 4, 5**). These proteins are specific cofactors for Rom2 and Tus1 respectively and are important for both the function and localization of these Rho1 GEFs: Rom2 function and localization are dependent on Ack1 but not on Rgl1; whereas Tus1 function and localization are dependent on Rgl1 but not on Ack1. The

localization mechanisms for the Rho1 GEFs are thus distinct, even when the localizations look superficially similar e.g., during secondary septum deposition late in cytokinesis.

These Ack1 and Rgl1 cofactors seem to differentially affect different subpopulations of each GEF, raising the possibility that other cofactors remain to be discovered. For example, Ack1 affects both the bud neck and the bud surface localizations of Rom2, but to different extents: the bud neck localizations of Rom2 (but not Tus1) are fully dependent on Ack1 whereas the bud surface localizations of Rom2 are largely, but not completely dependent on Ack1 (**Figs. 4, 5**). The residual localization of Rom2 to the bud surface in the absence of Ack1 helps explain why the phenotype of *ack1Δ* mutant cells is less severe than for *rom2Δ* cells. In the case of Rgl1, it seems partly required for the localization of Tus1 to the CAR but fully required for the subsequent septum localization of Tus1. Furthermore, Tus1 activated the Ycf1 lysosomal transporter. This activation seems to be independent of Rgl1 (our unpublished work), suggesting that Rgl1 may be a bud neck selective subunit of Tus1 signalling complexes.

The discovery of novel cofactors for the Rho1 GEFs adds a new layer of complexity to the regulation of the Rho1 GTPase. The study of these cofactors will shed light on the mechanisms that activate and target the Rho GEFs to different sub-cellular compartments and may even inform how these GEFs activate the appropriate subsets of available Rho effectors at each location. GEF cofactors may be a common aspect of GTPase switches, with some other examples are already known e.g., the CYK-4 cofactor for the Ect2 GEF of mammalian Rac GTPase (Yüce et al., 2005).

Overall, our analysis of Rom2 and Tus1 function reveals a surprising level of complexity in the spatio-temporal control of Rho1 and its effectors. The specialization of the different GEFs that act on a given GTPase is likely to be a universal aspect of Rho biology.

Materials & Methods

Media, chemicals, and transformation

The rich yeast medium (YPD) consisted of 1 % Bacto yeast extract (Difco), 2 % peptone (Difco), and 2 % glucose. Synthetic derived medium (SD, SGal/Suc) contained 0.67 % yeast nitrogen base without amino acids (Difco) and 2 % glucose, or 2 % galactose and 0.005 % sucrose respectively with the appropriate nutrient supplements and drug additions where appropriate. Solid media were as described above, with the addition of 2 % Bacto agar (Difco). Chemicals were from Sigma-Aldrich unless stated otherwise. Restriction enzymes were from New England Biolabs. All transformations were performed using the conventional lithium acetate method (Geitz et al., 1995).

Plasmids and yeast strains used

Plasmids and yeast strains used in this study are listed in **supplementary material Tables S4** and **S5** respectively. Double mutants were generated by mating two single mutant haploid strains of opposite mating type, selecting for the diploid, and then sporulating the diploid. The spores were dissected and double mutants were identified by marker analysis. In the case of the generation of *ack1rom2lrg1* and *rom1rom2lrg1*, *LRG1* was deleted from the parent strain using an *lrg1::LEU2* construct as previously described (Stewart et al., 2007).

Generation of pGAL-*ROM2*

The plasmid expressing full length *ROM2* under the control of the *GAL1,10* promoter was generated by inserting *ROM2* into the vector, pGREG535, by homologous recombination. This vector contains a *GAL1*,*10* promoter and a hemagglutinin tag (Jansen et al., 2005). The vector was digested with SalI to remove its HIS^+ marker. PCR amplified gene (using GregRom2F and GregRom2R) was cotransformed with SalI-digested pGREG535 into wild type yeast cells. Transformants were selected on SD-Leu plates. Plasmid DNA from five independent yeast colonies was transformed into XL1-Blue *Escherichia coli* cells (Stratagene). Plasmid DNA was purified, and the presence and orientation of an insert were confirmed by restriction digestion. The function of the plasmids was confirmed by *in vivo* complementation of the *rom2* mutant phenotypes.

Ycf1 Assay

The accumulation of red pigment in *ade2Δ* strains was measured essentially as described by Chaudhuri et al., 1997. 15 ml cell cultures were incubated overnight at 21 °C. The OD_{600} of each culture was taken and the same amount of cells were placed at 4 ˚C for 2 days to enhance the pigment development. All the cells were pelleted and resuspended in 500 ml 5% sulphosalicylic acid (Sigma) and lysed by bead beating. Lysates were centrifuged at high speed for 5 min. The supernatant removed and saved. The beads were washed with a further 500 ml 5% sulphosalicylic acid, centrifuged and the supernatant again removed. The OD_{530} was measured for the combined supernatants. The experiment was repeated three independent times.

Quantification of Glucan

The amount of glucan was estimated by aniline blue binding as described in Shedletzky et al., 1997. Cells were grown to mid-logarithmic phase, washed twice and resuspended in TE buffer to an OD_{600} 0.2 in a total volume of 500 ml. NaOH was added to a final concentration of 1N. The glucan was then solubilized by incubating the samples at 80ºC for 30 minutes. 2.1 ml aniline blue mix (0.03 % aniline blue, 0.18 N HCl, 0.49 M glycine/NaOH) was added and samples incubated at 50 ºC for 30 minutes and at room temperature for a further 30 minutes. Fluorescence was quantified using a spectrofluorimeter (400 nm excitation; 460 nm emission). All determinations were done four independent times.

The activity of glucan synthase was also estimated by quantifying the fraction of buds that stain positive for aniline blue in small-budded cells in cultures grown to mid-log phase in YPD and using a confocal microscope, as described by Sekiya-Kawasaki et al. (2002).

Determination of Pkc1 pathway activity

We determined the relative amount of basal Slt2 activation in cells using a *RLM1-LacZ* reporter construct (Jung et al., 2002) as described in Stewart et al (2007).

Synthetic Genetic Array Analysis

ROM2 and *TUS1* were individually deleted from the query strain and the SGA was performed as described by Tong et al., 2001.

Random Spore Analysis

The SGA positives were confirmed by random spore analysis using double heterozygous diploids taken during the SGA analysis according to Tong et al., 2001, but with additional selection for haploid spores as described by Rockmill et al., 1991. This extra selection step efficiently enriched for spores, bypassing the need to select against double heterozygous diploids. Spore suspensions were plated in SD medium lacking HIS (to select for MAT**a** haploids) and containing 200 μg/ml G418 to select for candidate knockouts, 100 μg/ml nourseothricin to select for query gene knockout, or both, to select for double mutant haploids. The plates were incubated for two to three days at 30°C and then colony growth was scored. An SSL interaction was confirmed where little or no colony growth appeared but only on the plates containing both G418 and nourseothricin,

Western blots

Wild type, *ack1*, and *ypl066w* were transformed with p*ROM2-13MYC* (from S. Yoshida). *ack1* and *ypl066w* cells were mated to *TUS1-13MYC* cells (from D. Pellman). The diploid cells were selected and dissected. *TUS1-13MYC, TUS1-13MYC ack1,* and *TUS1-13MYC ypl066w* cells and the transformants were grown in appropriate medium overnight. A 1:50 dilution was made with the overnight cultures and the freshly diluted cells were incubated for 3 hours at 21 ºC. One OD_{600} of cells were collected and resuspended in 100 μl 120 mM NaOH. This was incubated on ice for 15 minutes and then 30 μl of 5X sample buffer was added. The protein samples were boiled for 5 minutes. Any condensation was spun down and 30 μl was loaded on a 3-8 % Tris-Acetate gel (Invitrogen). The protein gel transfer and development of the immunoblot was as described in Krause & Gray, 2001. We used a mouse anti-MYC antibody from Calbiochem for the primary antibody and a sheep anti-mouse IgG-HRP antibody for the secondary from GE.

Microscopy: Image acquisition

Fluorescence images were acquired using a DeltaVision Core (Applied Precision) epifluorescence microscope fitted with an Olympus PlanApo 60x NA 1.4 objective, Chroma Technology Corporation filters, a CoolSNAP HQ CCD camera (Roper Scientific) and Applied Precision softWoRx suite imaging software (v4.0.0 release 16)

run on CentOS (release 4.7) operating system. The instrument controller ran version 5.40 sub a build 0113 software.

Live cell microscopy was performed by mounting cells in the appropriate pre-warmed media on 2.5% (w/v) agarose (Formedium) pads (made with the appropriate media). Still images consisting of Z-stacks (21 Z-sections, 0.2 micron spacing between planes) were acquired using the appropriate filter set and 3 second exposures for Tus1-GFP, Rom2-GFP and eCFP-Tub3 fusion proteins. Time lapse Z-stacks (comprising 18 Z-sections, 0.2 micron spacing between planes) were acquired every 1 minute for either 35 minutes (Tus1-GFP) or 45 minutes (Rom2-GFP) using 3 second exposures. Acquired fluorescence images were deconvolved with softWoRx using 15 iterations and the conservative algorithm (all other deconvolution parameters were set at their default values).

Microscopy: Analysis

Image data was processed/assembled using ImageJ v1.44m, Adobe Photoshop CS5 and Adobe illustrator CS5. Graphs were plotted using SigmaPlot v11.2.0.11 (SYSTAT).

Kymographs and montages were made from acquired time-lapse image sequences by reconstructing pixel data at the bud neck using the ImageJ (v1.44m) reslice command. Specifically, to generate kymographs, a range of Z-sections that spanned the bud neck region across all time points in acquired four dimensional (XYZT) time-lapse image sequences were subjected to a maximal intensity projection producing a three dimensional (XYT) image sequence. The reslice command (without interpolation) was then invoked from a straight line selection drawn adjacent and horizontal to the mother bud axis that was slightly longer than the bud neck width. Reslice output spacing was set to a value equivalent to the voxel depth (i.e. 0.2 microns), slice count was set at 5 (care being taken that this was sufficient in each case to encompass the 2-dimensional (XY) fluorescent signal at the bud neck at each time-point). The resulting stack of orthogonal slices was subjected to a maximal intensity projection and 90° CCW rotation to yield the resulting kymograph. Montages were generated using the same procedure, except the reslice command was invoked from straight line selections drawn on the native four dimensional time-lapse image sequence (XYZT).

Tus1-GFP and Rom2-GFP fluorescence intensity at the bud neck and bud tips respectively was measured using ImageJ v1.44m. A 3 pixel wide straight line or multi-segmented line was used to trace the fluorescent signal at the bud neck or bud tip respectively and the mean pixel intensity within its boundaries calculated. From this, mean background fluorescence across the same line positioned in the mother cell cytoplasm was subtracted. Measurements were performed on a single z-section within the stack that had the highest signal intensity.

Statistics

Statistical analyses were performed according to Cummings et al. (2007).

Acknowledgments

We thank the Pellman and Yoshida labs for their generous gift of reagents and Frank Holstege for sharing data prior to publication. This work was supported by the Biotechnology and Biological Sciences Research Council (BBSRC) grant BB/E011632/1 (to J.V.G.), by a BBSRC Ph.D. studentship (to M.C.) and a research grant from the Canadian Institutes of Health Research (to G.C.J.).

References

Andrews, P. D., and Stark, M. J. (2000) Dynamic, Rho1-dependent localization of Pkc1p to sites of polarized growth. *J. Cell Science* **113**, 2685-2693.

Ayscough, K. R., Eby, J. J., Lila, T., Dewar, H., Kozminski, K. G., and Drubin, D. G. (1999) Sla1 is a functionally modular component of the yeast cortical actin cytoskeleton required for correct localization of both Rho1p-GTPAse and Sla2p, a protein with Talin homology. *Mol. Biol. of the Cell* **10**, 1061-1999.

Audhya, A. and Emr, S. D. (2002) Stt4 PI 4-kinase localizes to the plasma membrane and functions in the Pkc1-mediated MAP kinase cascade. *Dev. Cell* **2**, 593-605.

Benschop, J. J., Brabers, N., van Leenen, D., Bakker, L. V., van Deutekom, H. W., van Berkum, N. L., Apweller, E., Lijnzaad, P., Holstege, F. C., and Kemmeren, P.

(2010) A consensus of core protein complex compositions for Saccharomyces cerevisiae. *Mol. Cell* **38**, 916-928.

Chaudhuri B., Ingavale, S., and Bachhawat, A. K. (1997) apd1+, a gene required for red pigment formation in ade6 mutants of Schizosaccharomyces pombe, encodes an enzyme required for glutathione biosynthesis: a role for glutathione and a glutathione-conjugate pump. *Genetics* **145**, 75–83.

Cherfils, J., and Zeghouf, M. (2011) Chronicles of the GTPase switch. *Nat. Chem. Biol.* **7**, 493-495.

Connolly, B. A., Rice, J., Feig, L. A., and Buchsbaum, R. J. (2005) Tiam1-IRSp53 complex formation directs specificity of rac-mediated actin cytoskeleton regulation. *Mol. Cell Biol.* **25**, 4602-4614.

Cumming, G., Fidler F,, and Vaux, D. L. (2007) Error bars in experimental biology. *J Cell Biol*. **177**, 7-11.

Garcia-Mata, R. and Burridge, K. (2007) Catching a GEF by its tail. *Trends Cell Biol.* **17**, 36-43.

Gietz, R. D., Scheistl, R. H., A. R. Wellems, A. R., and Woods, R. A. (1995) Studies on the transformation of intact yeast cells by the LiAc/SS-DNA/PEG procedure. *Yeast* **11**, 355-360.

Hillenmeyer, M. E., Fung, E., Wildenhain, J., Pierce, S. E., Hoon, S. et al. (2008) The chemical genomic portrait of yeast: uncovering a phenotype for all genes. *Science* **18**, 362-365.

Ho, H. L., Lee, H. Y., Liao, H. C., and Chen, M. Y. (2008) Involvement of Saccharomyces Avo3p/Tsc11p in maintaining TOR complex 2 integrity and coupling to downstream signaling. *Eukaryot. Cell* **7**, 1328-1343.

Huh, W. K., Falvo, J. V., Gerke, L. C., Carroll, A. S., Howson, R. W., Weissman, J. S., and O'Shea, E. K. (2003) Global analysis of protein localization in budding yeast. *Nature* **425**, 686-691.

Jansen, G., Wu, C., Schade, B., Thomas, D. Y., and Whiteway, M. (2005) Drag & drop cloning in yeast. *Gene* **344**, 43-51.

Jung, U. S., Sobering, A. K., Romeo, M. J., and Levin, D. E. (2002) Regulation of the yeast Rlm1 transcription factor by the Mpk1 cell wall integrity MAP kinase. *Mol. Microbiol.* **46**, 781-789.

Kobayashi, T., Takematsu, H., Yamaji, T., Hiramoto, S., and Kozutsumi, Y. (2005) Disturbance of sphingolipid biosynthesis abrogates the signaling of Mss4, phosphatidylinositol-4-phosphate 5-kinase, in yeast. *J. Biol. Chem.* **280**, 18087-18094.

Kono, K., Nogami, S., Abe, M., Nishizawa, M., Morishita, S., Pellman, D., and Ohya, Y. (2008) G1/S cyclin-dependent kinase regulates small GTPase Rho1p through phosphorylation of RhoGEF Tus1p in Saccharomyces cerevisiae. *Mol. Biol. Cell* **19**, 1763-1771.

Krause, S. A., Xu, H., and Gray, J. V. (2008) The synthetic genetic network around PKC1 identifies novel modulators and components of protein kinase C signaling in Saccharomyces cerevisiae. *Eukaryot. Cell* **7**, 1880-1887.

Lesage, G., Shapiro, J., Specht, C.A., Sdicu, A.M., Ménard, P. et al. (2005) An interactional network of genes involved in chitin synthesis in Saccharomyces cerevisiae. *BMC Genet.***16**, 6-8.

Levin, D. E. (2005) Cell wall integrity signaling in Saccharomyces cerevisiae. *Microbiol. Mol. Biol. Rev.* **69**, 262-291.

Logan, M. R., Jones, L., and Eitzen, G. (2010) Cdc42p and Rho1p are sequentially activated and mechanistically linked to vacuole membrane fusion. *Biochem. Biophys. Res. Commun.* **394**, 64-69.

Manning, B. D., Padmanabha, R., and Snyder, M. (1997) The Rho-GEF Rom2p localizes to sites of polarized cell growth and participates in cytoskeletal functions in Saccharomyces cerevisiae. *Mol. Biol. Cell* **8**, 1829-18-44.

Mutoh, T., Nakano, K., and Mabuchi, I. (2005) Rho1-GEFs Rgf1 and Rgf2 are involved in formation of cell wall and septum, while Rgf3 is involved in cytokinesis in fission yeast. *Genes Cells* **10**, 1189-1202.

Ozaki, K., Tanaka, K., Imamura, H., Hihara, T., Kameyama, T., Nonaka, H., Hirano, H., Matsuura, Y., and Takai, Y. (1996) Rom1p and Rom2p are GDP/GTP exchange proteins (GEPs) for the Rho1p small GTP binding protein in Saccharomyces cerevisiae. *EMBO J.* **15**, 2196-2207.

Paumi, C.M., Menendez, J., Arnolodo, A., Engels, K., Iyer, K. R., Thaminy, S., Georgiev, O., Barral, Y., Michaelis, S., and Stagljar, I. (2007) Mapping protein-protein interactions for the yeast ABC transporter Ycf1p by integrated split-ubiquitin membrane yeast two-hybrid analysis. *Mol. Cell* **26**, 15-25.

Pertz, O. Hodgson, L., Klemke, R. L., and Hahn, K. M. (2006) Spatiotemporal dynamics of RhoA activity in migrating cells. *Nature* **440**, 1069-1072.

Pertz, O. (2010) Spatio-temporal Rho GTPase singaling – where are we now? *J. Cell Sci.* **123**, 1841-1850.

Petkova, M. I., Pujol-Carrion, N., Arroyo, J., Garcia-Catalejo, J., and Angeles de la Torre-Ruiz, M. (2010) Mtl1 is required to activate general stress response through Tor1 and Ras2 inhibition under conditions of glucose starvation and oxidative stress. *J. Biol.Chem.* **285**, 19521-19531.

Piekney, A., Wener, M., and Glotzer, M. (2005) Cytokinesis: Welcome to the Rho zone. *Trends Cell Biol.* **15**, 651-658.

Roberts, C. J., Nelson, B., Marton, M. J., Stoughton, R., Meyer, M. R., Bennett, H. A., He, Y. D., Dai, H., Walker, W. L., Hughes, T. R. et al. (2000) Signaling and circuitry of multiple MAPK pathways revealed by a matrix of global gene expression profiles. *Science* **287**, 873-880.

Rockmill, B., Lambie, E. J., and Roeder, G. S. (1991) Spore enrichment. *Methods Enzymol.* **194**, 146-149.

Rossman, K. L., Der, C. J., and Sondek, J. (2005) GEF means go: Turning on RHO GTPases with guanine nucleotide exchange factors. *Nat. Rev. Mol. Cell Biol.* **6**, 167-180.

Sahai, E, and Marshall, C. J. (2002) RHO-GTPases and cancer. *Nat. Rev. Cancer* **2,** 133-142.

Schmelzle, T., Helliwell, S. B., and Hall, M. N. (2002) Yeast protein kinases and the RHO1 exchange factor TUS1 are novel components of the cell integrity pathway. *Mol. Cell. Biol.* **22**, 1329-1339.

Schmidt, A., Bickle, M., Beck, T., and Hall, M. N. (1997) The yeast phosphatidylinositol kinase homolog TOR2 activates RHO1 and RHO2 via the exchange factor ROM2. *Cell* **88**, 531-542.

Schmidt, A, Schmelzle, T, and Hall MN. (2002) The RHO1-GAPs SAC7, BEM2 and BAG7 control distinct RHO1 functions in *Saccharomyces cerevisiae*. *Mol Microbiol.* **45**, 1433-1441.

Sekiya-Kawasaki, M., Abe, M., Saka, A., Wantanabe, D., Kono, K., Minemura-Askawa, M., Ishihara, S., Wantanabe, T., and Ohya, Y. (2002) Dissection of upstream regulatory components of the Rho1p-effector, 1,3-beta-glucan synthase, in *Saccharomyces cerevisiae*. *Genetics* **162**, 663-676.

Shedletzky, E., Unger, C., and Delmar, D. P. (1997) A microtiter-based fluorescence assay for (1,3)-beta-glucan synthases. *Anal. Biochem.* **15**, 88-93.

Stewart, M. S., Krause, S. A., McGhie, J., and Gray, J. V. (2007) Mpt5p, a stress tolerance- and lifespan-promoting PUF protein in Saccharomyces cerevisiae, acts upstream of the cell wall integrity pathway. *Eukaryot. Cell* **6**, 262-270.

Struckhoff, A. P., Rana, M. K., and Worthylake, R. A. (2011) RhoA can lead the way to tumor invasion and metastasis. *Front. Biosci*. **16**, 1915-1925.

Taira, K., Umikawa, M., Takei, K., Myagmar, B. E., Shinzato, M., Machida, N., Uetzato, H., Nonaka, S., and Kariya, K. (2004) The Traf2- and Nick-interacting kinase as a putative effector of Rap2 to regulate actin cytoskeleton. *J. Biol. Chem.* **279**, 49488-49496.

Takaki, T., Trenz, K., Costanzo, V., and Petronczki, M. (2008) Polo-like kinase 1 reaches beyond mitosis-cytokinesis, DNA damage response, and development. *Curr. Opin. Cell Biol.* **20**, 650-660.

Tolliday, N., VerPlank, L., and Li, R. (2002) Rho1 directs fomin-mediated actin ring assembly during budding yeast cytokinesis. *Curr. Biol.* **12**, 1864-1870.

Tong, A. H., Evangelista, M., Parsons, A. B., Xu, H., Bader, G. D., Page, N., Robinson, M., Raghibizadeh, S., Hogue, C. W., Bussey, H., et al. (2001) Systematic genetic anaylsis with ordered arrays of yeast deletion mutants. *Science* **294**, 2364-2368.

Tong, A. H., Lesage, G., Bader, G. D., Ding, H., Xu, H., Xin, X., Young, J., Berriz, G. F., Brost, R. L., Chang, M., et al. (2004) Global mapping of the yeast genetic interaction network. *Science* **303**, 808-813.

Van Driessche, B., Tafforeau, L., Hentges, P., Carr, A.M., and Vandenhaute, J. (2005) Additional vectors for PCR-based gene tagging in Saccharomyces cerevisiae and Schizosaccharomyces pombe using nourseothricin resistance. *Yeast* **22**, 1061-1068.

Wolfe, B. A., and Glotzer, M. (2009) Single cells (put a ring on it). *Denes Dev.* **23**, 896-901.

Yoshida, S., Kono, K., Lowery, D. M., Bartolini, S., Yaffe, M. B., Ohya, Y., and Pellman, D. (2006) Polo-like kinase Cdc5 controls the local activation of Rho1 to promote cytokinesis. *Science* **313**, 108-111.

Yoshida, S., Bartolini, S., and Pellman, D. (2009) Mechanisms for concentrating Rho1 during cytokinesis. *Genes Dev.* **23**, 810-823.

Yüce, O, Piekny, A, and Glotzer, M. (2005) An ECT2-centralspindlin complex regulates the localization and function of RhoA. *J Cell Biol.* **170**, 571-82.

Figure Legends

Fig. 1. The Rho1-GEFs, Rom2 and Tus1, differentially affect Rho1-effector pathways. (A) Ycf1 activity was determined in wild-type, *rom2* and *tus1* mutants. We generated the double mutants, *rom2 ade2* and *tus1 ade2,* and compared the amount of red pigmentation relative to an *ade2* single mutant, where Ycf1 activity is required to acquire the red pigment in *ade2* mutants. The differences observed between *ade2* and *rom2 ade2* tus1 ade2 are significant ($0.05>p>0.01$ and $p<0.001$ respectively). Note: for wild type cells, n=4; for *ade2* cells, n=15; for *ade2rom2* cells, n=6; and for *ade2tus1* cells, n=4. The error bars shown represent standard error and we used student t-test to determine statistical significance. (**B)** Glucan levels were determined in wild-type, *rom2* and *tus1* cells using the fluorochrome aniline blue which complexes with 1,3-β-glucan. The amount of fluorescence was determined for each mutant relative to the amount for the congenic wild type strain. There was no significant difference between the levels found in wild type cells and *tus1* mutant cells ($p > 0.1$); the difference between wild type and *rom2* cells was significant ($0.05>p <>0.01$). For all cell types, n=4. The error bars shown represent standard error and statistical significance was calculated using the student t-test. **(C)** Wild type, *rom2* and *tus1* cells were stained with aniline blue and the percentage of stained buds in small-budded cells was determined. The percentage of small buds stained in *rom2* mutant cells were significantly less than that observed in wild type cells ($0.01>p>0.001$). The difference between wild type and *tus1* cells was not significant ($p>0.1$). For all cell types, n=3. The error bars shown represent standard error and statistical significance was determined using the student t-test.

Fig. 2. Rom2 and Tus1 have opposite affects on the Rho1-Pkc1 signalling pathway. (A) *rom2* and *tus1* and congenic wild type strains were transformed with a Rlm1-*LacZ* reporter construct and logarithmically growing cultures were assayed for β-galactosidase activity. The relative reporter activity of a mutant was determined relative to congenic wild type cells. In *rom2* mutant cells, the relative activity of the reporter construct was significantly low ($p < 0.001$); whereas the relative activity in *tus1* cells was significantly high ($p < 0.05$). Note: for wild type cells, n=28; for *rom2* cells, n=12; and for *tus1* cells, n=13. The error bars shown represent standard error and statistical significance was

calculated using the student t-test. (**B)** Wild type strains were transformed with a Rlm1-*LacZ* reporter and either a vector, pGAL-*ROM2*, or pGAL-*TUS1* and relative reporter activity determined as described above. Overexpression of *ROM2* enhanced relative reporter activity ($p<0.001$); whereas overexpression of *TUS1* inhibited it ($p<0.001$). Note: for wild type cells expressing an empty vector, n=26; for wild type cells overexpressing *ROM2*, n=22; and for wild type cells overexpressing *TUS1*, n=7. The error bars shown represent standard error and statistical significance was calculated using the student t-test. (**C)** *rom1tus1* and *rom2tus1* double mutants were generated and transformed with a Rlm1-*LacZ* reporter construct and relative reporter activity for the double mutants was determined as above and compared to those of the single mutants. The observed reporter activity levels in the double mutants, *rom1tus1* and *rom2tus1*, was significantly higher than in the single *rom1* ($0.001<p<0.01$) or *rom2* ($p<0.001$) mutant, but lower than in the single *tus1* mutant ($0.01<p<0.05$ and $p<0.001$ respectively). Note: for wild type cells, n=28; for *rom2* cells, n=12; for *tus1* cells, n=13; for *rom1* cells, n=9; for *rom2tus1*, n=4; and for *rom1tus1* cells, n=6. The error bars shown represent standard error and statistical significance was calculated using the student t-test.

Fig. 3. The Synthetic Genetic Interaction Networks of *ROM2* and *TUS1* are largely distinct. (A) *ROM2* or *TUS1* genes were deleted from the SGA query strain as described by Tong et al., 2000. SGA analysis was performed separately on each null mutant. The positives were confirmed by random spore analysis (and also by tetrad analysis in some cases) (see **supplementary material online**). A set diagram showing the extent of overlap between the two networks is shown. The Rho1-Pkc1 signalling pathway is displayed with (**B**) *ROM2* and (**C**) *TUS1* genetic interactors highlighted in bold and underlined respectively.

Fig. 4. The Spatial and temporal pattern of Tus1-GFP localization in *ypl066w* cells. (**A)** Tus1-GFP localization is shown in an otherwise wild type background expressing N-terminal eCFP-tagged Tub3 which marks the spindle pole body (SPB) and the mitotic spindle. The image series is a composite of cells representative of the distinct phases of localization. Scale bars = 2 μm. **(B)** Average intensity projection images of representative *ypl066w* cells co-expressing Tus1-GFP and eCFP-Tub3 (note: 'split band' and 'signal at

cell separation' categories were not observed in *ypl066w* cells). Scale bars = 2 μm. (**C)** Histogram of wild type (n=209), *ypl066w* (n=170) and *ack1* (n=144) cells co-expressing Tus1-GFP and eCFP-Tub3. All cells included in the sampling were post-mitotic spindle breakdown with two visible spindle pole bodies. (**D)** Wild type and *ypl066w* cells expressing Tus1-GFP were mixed in a 1:1 ratio and the fluorescence intensity of the GFP signal at the bud neck in cells following spindle breakdown was measured in the same field of vision (specifically, only cells with the 'band (no septum)' category signal were measured). The *ypl066w* cells were marked by co-expression of eCFP-Tub3 (wild type cells harboured an 'empty' vector (eV) instead).

Fig. 5. The Spatial and temporal pattern of Rom2-GFP localization in *ack1* cells. **(A)** Rom2-GFP localization in a wild type background expressing N-terminal eCFP tagged Tub3. The image series is a composite of cells representative of the distinct phases of localization. All images are average intensity projections. Scale bars = 2 μm. **(B)** Average intensity projection images of representative *ack1*Δ cells co-expressing Rom2-GFP and eCFP-Tub3. Scale bars = 2 μm. **(C)** Histogram of post-anaphase wild type (n=181), *ack1* (n=155) and *ypl066w* (n=223) cells co-expressing Rom2-GFP and eCFP-Tub3 and scored for Rom2-GFP bud neck signals. (**D)** Wild type and *ack1* cells expressing Rom2-GFP were mixed in a 1:1 ratio and the fluorescence intensity of the GFP signal at bud tips in small budded cells with a single spindle pole body was measured in the same field of vision. The *ack1* cells were marked by eCFP-Tub3 expression (wild type cells harboured an 'empty' vector (eV) instead). **(E)** Histogram of wild type, *ack1* and *ypl066w* cells co-expressing Rom2-GFP and eCFP-Tub3 and scored for Rom2-GFP bud tip signals at the cell cycle stages indicated.

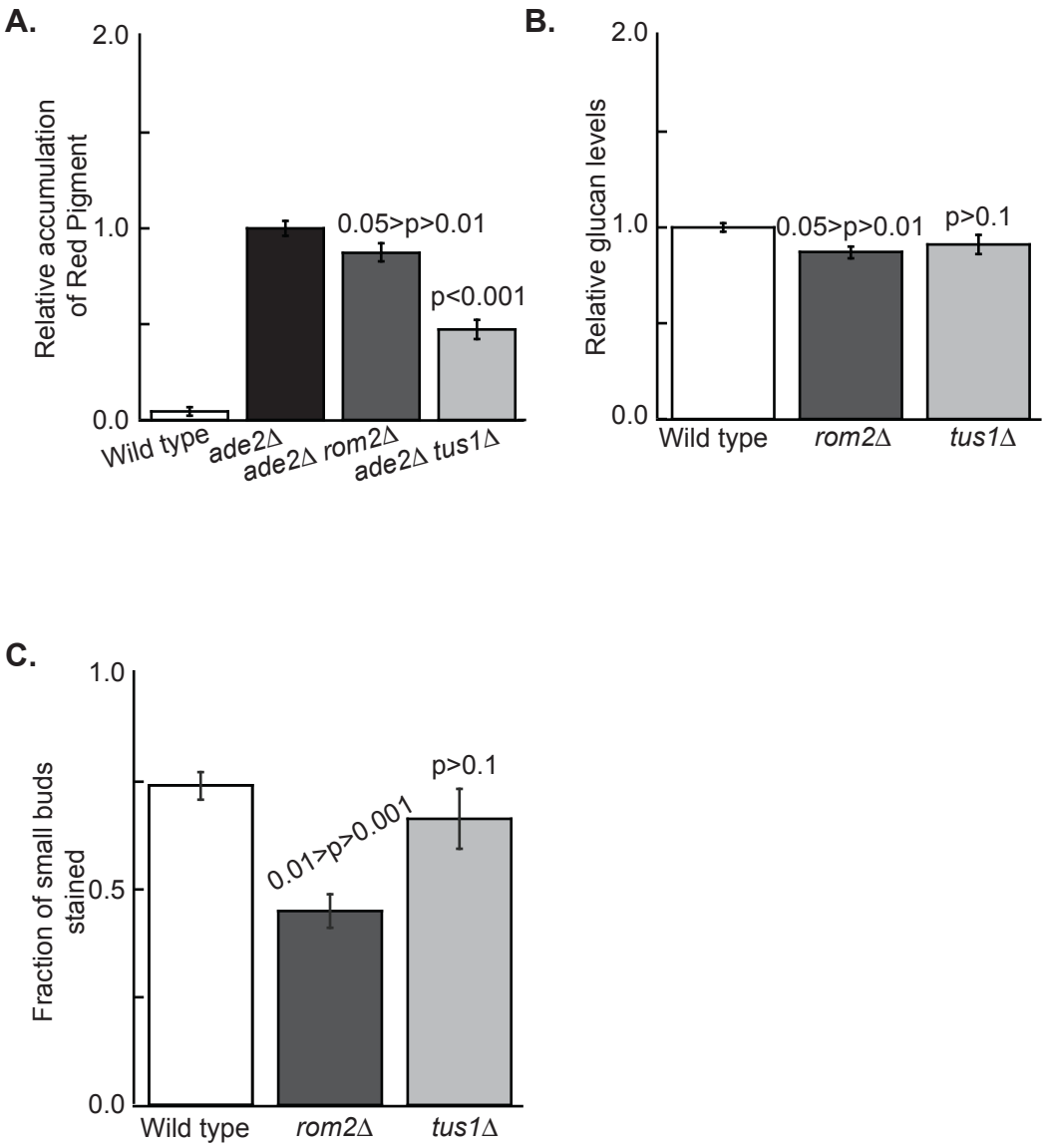
A.
Relative accumulation of Red Pigment
2.0
1.0
0.0
0.05>p>0.01
p<0.001
Wild type
ade2Δ
ade2Δ rom2Δ
ade2Δ tus1Δ
B.
Relative glucan levels
2.0
1.0
0.0
0.05>p>0.01
p>0.1
Wild type
rom2Δ
tus1Δ
C.
Fraction of small buds stained
1.0
0.5
0.0
0.01>p>0.001
p>0.1
Wild type
rom2Δ
tus1Δ

Figure 1

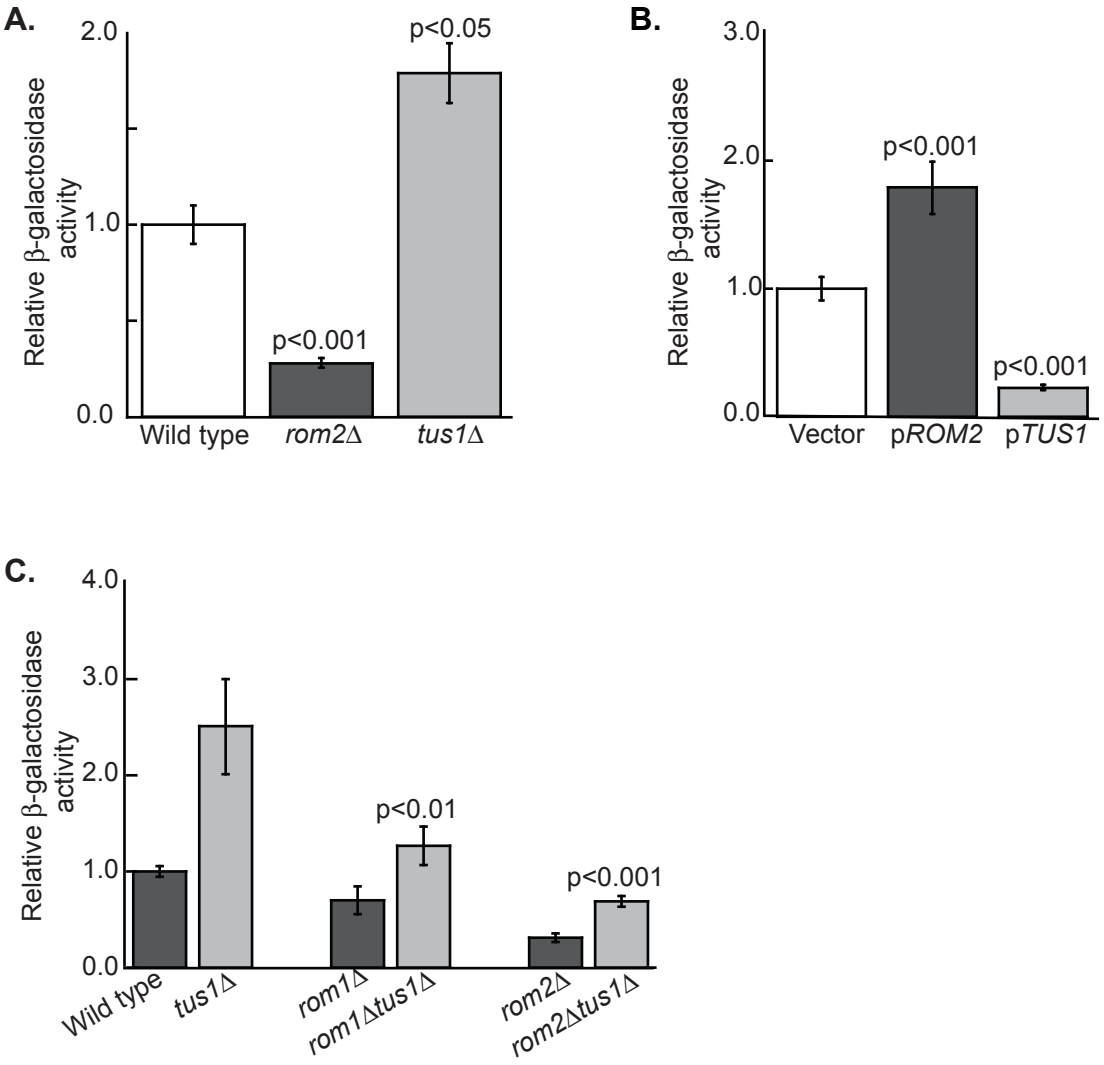
A.
Relative β-galactosidase activity
2.0
1.0
0.0
p<0.05
p<0.001
Wild type
rom2Δ
tus1Δ
B.
Relative β-galactosidase activity
3.0
2.0
1.0
0.0
p<0.001
p<0.001
Vector
pROM2
pTUS1
C.
Relative β-galactosidase activity
4.0
3.0
2.0
1.0
0.0
p<0.01
p<0.001
Wild type
tus1Δ
rom1Δ
rom1Δtus1Δ
rom2Δ
rom2Δtus1Δ

Figure 2

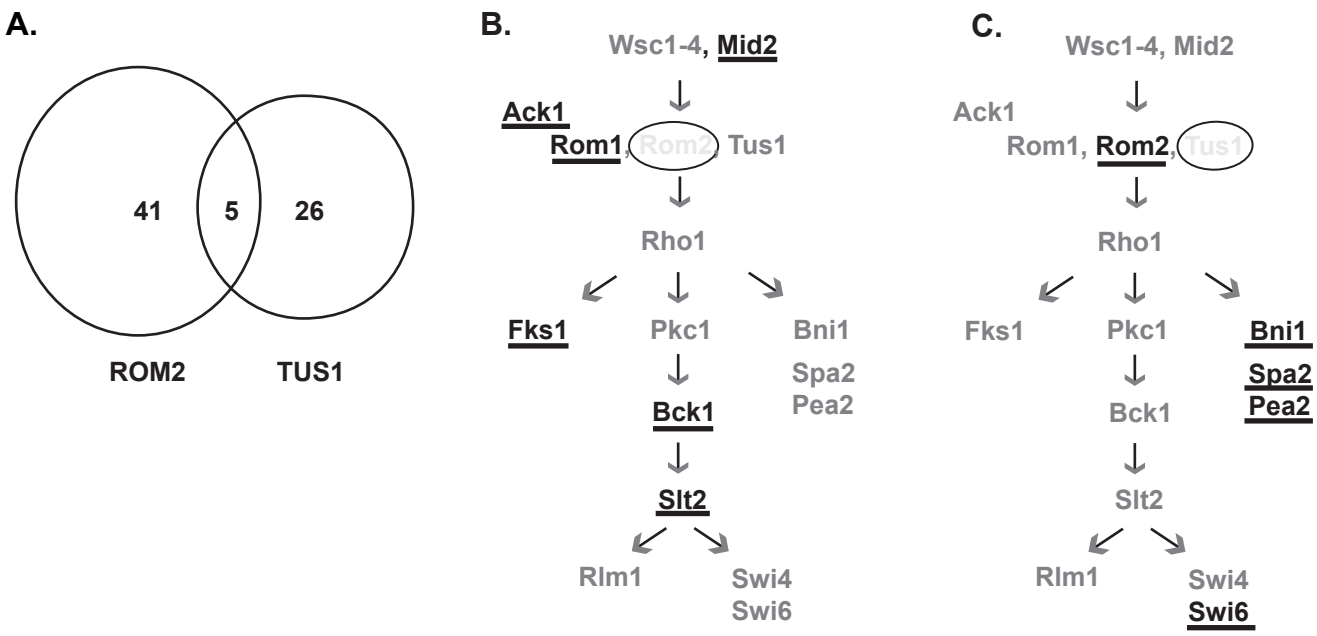
A.
41
5
26
ROM2
TUS1
B.
Wsc1-4, Mid2
Ack1
Rom1, Rom2, Tus1
Rho1
Fks1
Pkc1
Bni1
Spa2
Pea2
Bck1
Slt2
Rlm1
Swi4
Swi6
C.
Wsc1-4, Mid2
Ack1
Rom1, Rom2, Tus1
Rho1
Fks1
Pkc1
Bni1
Spa2
Pea2
Bck1
Slt2
Rlm1
Swi4
Swi6

Figure 3

A. *TUS1-GFP*

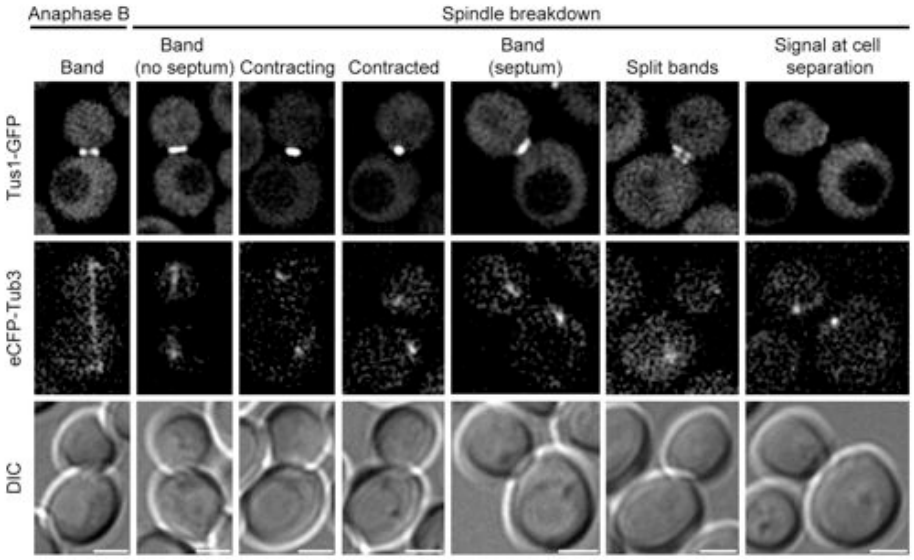

B. *TUS1-GFP ypl066wΔ*

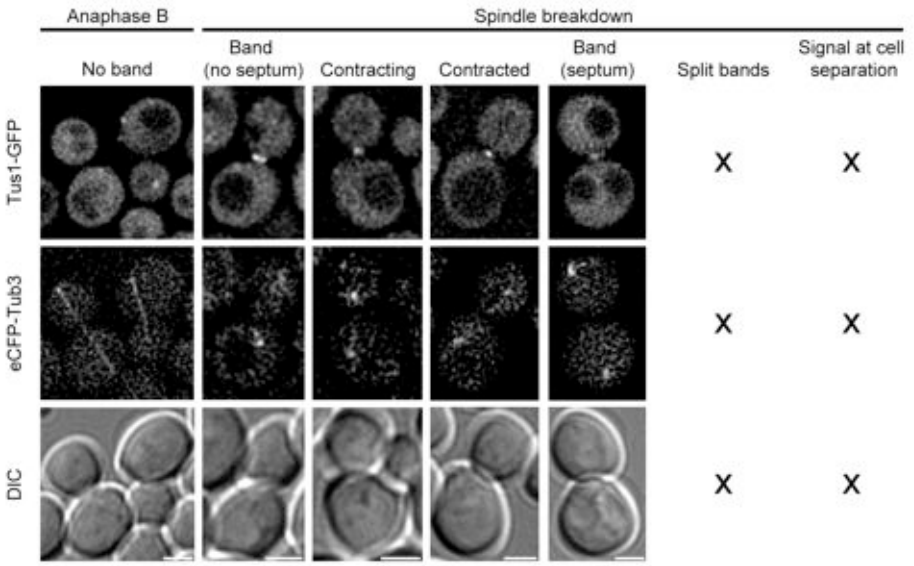

C.

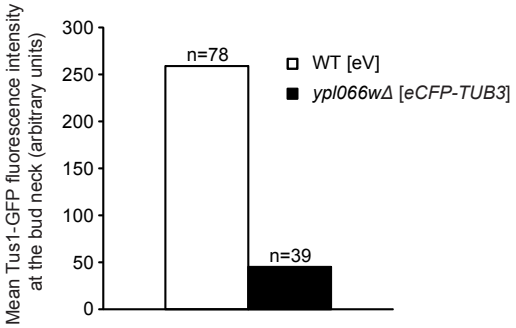

D.

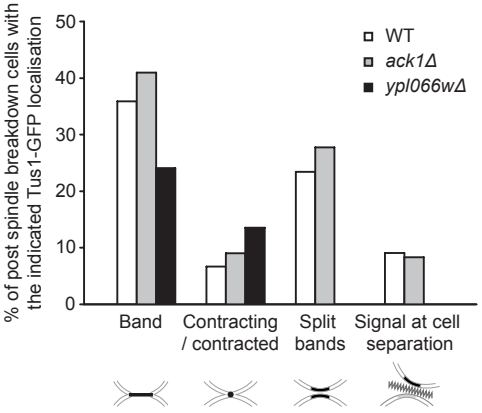

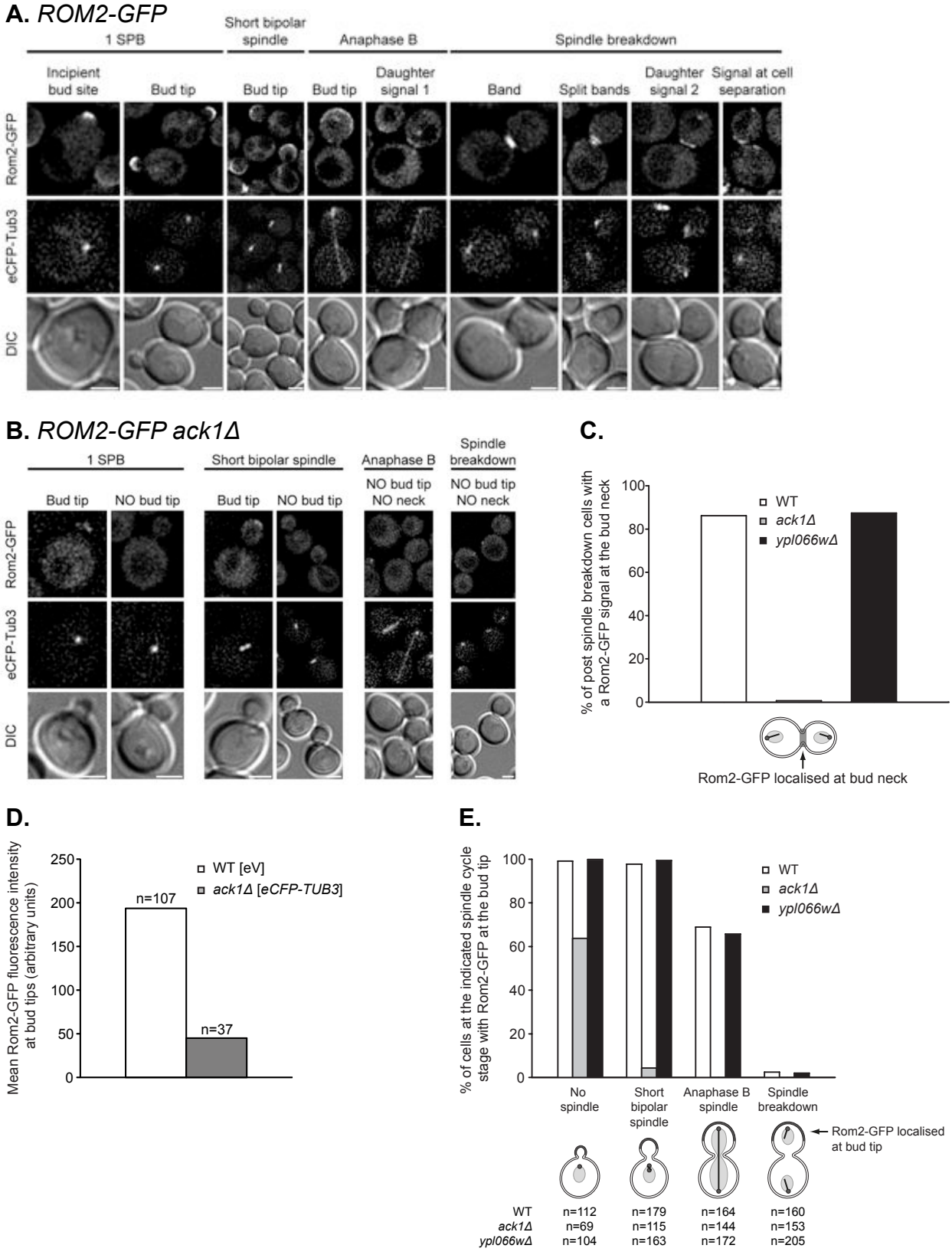
A. ROM2-GFP
1 SPB
Short bipolar spindle
Anaphase B
Spindle breakdown
Incipient bud site
Bud tip
Bud tip
Bud tip
Daughter signal 1
Band
Split bands
Daughter signal 2
Signal at cell separation
Rom2-GFP
eCFP-Tub3
DIC
B. ROM2-GFP ack1Δ
1 SPB
Short bipolar spindle
Anaphase B
Spindle breakdown
Bud tip
NO bud tip
Bud tip
NO bud tip
NO bud tip NO neck
NO bud tip NO neck
Rom2-GFP
eCFP-Tub3
DIC
C.
% of post spindle breakdown cells with a Rom2-GFP signal at the bud neck
100
80
60
40
20
0
WT
ack1Δ
ypl066wΔ
Rom2-GFP localised at bud neck
D.
Mean Rom2-GFP fluorescence intensity at bud tips (arbitrary units)
250
200
150
100
50
0
WT [eV]
ack1Δ [eCFP-TUB3]
n=107
n=37
E.
% of cells at the indicated spindle cycle stage with Rom2-GFP at the bud tip
100
80
60
40
20
0
WT
ack1Δ
ypl066wΔ
No spindle
Short bipolar spindle
Anaphase B spindle
Spindle breakdown
Rom2-GFP localised at bud tip
WT n=112 n=179 n=164 n=160
ack1Δ n=69 n=115 n=144 n=153
ypl066wΔ n=104 n=163 n=172 n=205

Supplemental Material

Supplementary Movie Legends:

Movie S1. Tus1-GFP time lapse. Movie (4 frames/sec) constructed from the image series presented in Supplemental Figure 2A.

Movie S2. Rom2-GFP time lapse. Movie (4 frames/sec) constructed from the image series presented in Supplemental Figure 3A.

Supplementary Table Legends

Table S1. Synthetic genetic array results for *rom2*. *ROM2* was deleted from the query strain and the SGA (n=3) was performed as described by Tong et al., 2001. The positives that were found in 2 or all 3 screens were then confirmed using random spore analysis.

Table S2. Synthetic genetic array results for *tus1*. *TUS1* was deleted from the query strain and the SGA (n=3) was performed as described by Tong et al., 2001. The positives that were found in 2 or all 3 were then confirmed using random spore analysis.

Table S3. Summary of genetic interactions between *ACK1, RGL1/YPL066W* and the Rho1 GEF genes.

Synthetic lethal interactions are marked with a minus sign (-, inviable double mutants), viable combinations with a plus sign (+, viable double mutants).

Table S4. List of plasmids used in this study.

Table S5. List of yeast strains used in this study. All yeast strains are in the yeast deletion background (BY4741).

Supplementary Figure Legends:

Fig. S1. Suppression of Rho1-Gef mutants. (A) Wild type**,** *rom2 and tus1* strains were transformed with a vector control, p*ROM2*, or p*TUS1*. The transformed strains were tested for their sensitivity by serial dilutions on SD-URA plates containing either 20 μg/ml benomyl or 200 μg/ml chlorpromazine. Overexpression of *TUS1* in a *rom2* mutant suppresses its sensitivity to benomyl. Overexpression of *ROM2* in a *tus1* mutant suppresses the chlorpromazine sensitivity of *tus1* mutants. "+" = growth. "-" = no growth. (**B)** *rom1rom2* mutants containing a *URA3*-marked *ROM2* plasmid (p*ROM2)* to maintain viablity were transformed with a vector control, pGAL-*ROM2*, or pGAL-*TUS1*. The transformed cells were treated with 5-FOA to select for loss of the p*ROM2* plasmid. However, only the pGAL-*ROM2* containing strain was able to lose the p*ROM2* plasmid, indicating that Tus1 cannot suppress the viablity defect of a *rom1rom2* double mutant.

Fig. S2. Time-lapse localization of Tus1-GFP. (**A**) Maximum intensity projection images in the X-Y plane are shown from a representative single cell expressing Tus1-GFP in a wild type background are shown. Images were collected over 35 minutes at 1 minute intervals and the scale bar is 2 μm. The asterix marks the beginning of the second phase localization signal and arrows indicate the two separate ring structures that are subsequently observed. (**B**) Time lapse series of three representative individual cells (n=38) presented as kymographs (scale bar = 3.5 min) and (**C**) as a montage (looking through the bud neck at consecutive time points). Numbers to the left and right refer to the time of image capture within the 35 min series.

Fig. S3. Time-lapse localization of Rom2-GFP. (**A**) Maximum intensity projection images in the X-Y plane are shown from two representative single cells within the same field of vision expressing Rom2-GFP in a wild type background are shown. Images were collected over 45 minutes at 1 minute intervals and the scale bar is 2 μm. (**B**) Time lapse series of three representative individual cells (n=41) presented as kymographs (scale bar = 4.5 min) and (**C**) as a montage (looking through the bud neck at consecutive time points). Numbers to the left and right refer to the time of image capture within the 45-minute series.

Fig. S4. Ack1 and Ypl066w act via Rom2 and Tus1 respectively. (A) Overexpression of *ACK1* does not elevate the Pkc1 signalling defect in a *rom2* mutant. Congenic wild type and *rom2* cells were transformed with the Rlm1-*LacZ* reporter construct and either a vector control or pGAL-*ACK1*. β-galactosidase activity was assayed in the transformants. The difference observed between the vector control and pGAL-*ACK1* in *rom2* mutant cells is not significant (n=3: $p>0.1$). (**B**) Overexpression of *TUS1* does not alter the observed high activity levels of Pkc1 signalling in a *ypl066w* mutant. Congenic wild type and *ypl066w* cells were transformed with the Rlm1-*LacZ* reporter construct and either a vector control or pGAL-*TUS1*. β-galactosidase activity was assayed in the transformants. The difference observed between the vector and pGAL-*TUS1* in *ypl066w* mutant cells is not significant (n=3: $p>0.1$). All error bars shown represent Standard Error and statistical significance was determined by the student t-test.

Fig. S5. Localization of Tus1 is Ack1 independent. Localization of Tus1-GFP is normal in an *ack1* mutant. Average intensity projection images of representative anaphase and post-anaphase *ack1* cells co-expressing Tus1-GFP and the eCFP-Tub3 tubulin marker are shown. Scale bars = 2 μm.

Fig. S6. Rom2 localization is not dependent on Ypl066w. (**A**) Localization of Rom2-GFP is mainly unaltered in a *ypl066w* mutant. Average intensity projection images of representative *ypl066w* cells co-expressing Rom2-GFP and the eCFP-Tub3 tubulin marker are shown. Scale bars = 2 μm. (**B**) Quantification of Rom2-GFP localization in post-anaphase *ypl066w* cells.

Fig. S7. The levels of the Rho1-GEFs are not altered in *ack1* or *ypl066w* mutants. (**A**) The steady state level of Rom2 protein was determined in wild type, *ack1*, and *ypl066w* cells. Strains were transformed with a p*ROM2-13MYC* plasmid. The cells were selected and grown to log phase and subject to Western blotting for the MYC epitope. A cross-reacting band also present in untransformed cells is shown as a loading control. (**B**) The steady state level of Tus1 protein was determined by Western blot analysis in wild-type, *ack1* and *ypl066w* cells. Strains were mated to *TUS1-13MYC* cells. The diploid cells were selected and dissected. Wild-type *TUS1-13MYC*, *TUS1-13MYC ack1* and

TUS1-13MYC ypl066w cells were grown to log phase before protein was extracted and subjected to Western blotting. A cross-reacting band is shown as a loading control.

Table S1: SSL genetic interaction network around *ROM2*

ORF	Gene Name
YBL058W	SHP1
YCL007C	VMA9
YDL185W	TFP1
YDL203C	ACK1
YDL232W	OST4
YDR017C	KCS1
YDR027C	VPS54
YDR174W	HMO1
YDR176W	NGG1
YDR207C	UME6
YDR245W	MNN10
YDR417c	YDR417c
YER167W	BCK2
YGL084C	GUP1
YGL200C	EMP24
YGR070W	ROM1
YGR252W	GCN5
YHL025W	SNF6
YHR030C	SLT2
YIL153W	RRD1
YIR023W	DAL81
YJL095W	BCK1
YJL124C	LSM1
YJL140W	RPB4
YJL175W	YJL175W
YJL183W	MNN11
YJR073C	OPI3
YJR118C	ILM1
YKL139W	CTK1
YLR332W	MID2
YLR342W	FKS1
YML016C	PPZ1
YMR003W	AIM34
YMR186W	HSC82
YMR274C	RCE1
YNL064C	YDJ1
YNR052C	POP2
YOL081W	IRA2
YOR035C	SHE4
YOR251C	TUM1
YOR332W	VMA4
YPL031C	PHO85
YPL101W	ELP4
YPL268W	PLC1
YPR023C	EAF3

Table S2: SSL genetic interaction network around *TUS1*

ORF	Gene Name
YDL232W	OST4
YDR017C	KCS1
YDR432W	NPL3
YEL064C	AVT2
YEL067C	YEL067C
YER101C	AST2
YER119C-A	AVT6
YER149C	PEA2
YER153C	PET122
YFL014W	HSP12
YGL045W	RIM8
YHR111W	UBA4
YIL008W	URM1
YJL159W	HSP150
YLL021W	SPA2
YLR182W	SWI6
YLR330W	CHS5
YLR371W	ROM2
YLR384C	IKI3
YLR393W	ATP10
YMR003W	AIM34
YMR063W	RIM9
YMR116C	ASC1
YMR124W	YMR124W
YMR228W	MTF1
YMR274C	RCE1
YMR312W	ELP6
YNL271C	BNI1
YPL031C	PHO85
YPL086C	ELP3
YPL101W	ELP4

Table S3. Synthetic lethal genetic interactions

	rom1	*rom2*	*tus1*	*ack1*	*ypl066w*
rom1	NA	-	+	+	ND
rom2	-	NA	+	-	+
tus1	+	+	NA	+	+
ack1	+	-	+	NA	+
ypl066w	ND	+	+	+	NA

NA=not applicable
ND=not determined

Table S4: Plasmids used.

Name of Plasmid	Reference
pGREG535	Euroscarf (Jansen et al., 2005)
p*Rlm1-LacZ*	D. Levin (Jung et al., 2002)
pGAL-*TUS1*	Krause et al., 2008
pGAL-*ACK1*	Krause et al., 2008
pGAL-*ROM2*	This study
p*ROM2-13MYC*	S. Yoshida (Yoshida et al., 2006)
p*ROM2*	M. Hall (Schmidt et al., 1997)
p*TUS1*	M. Hall (Schmelzle et al., 2002)
p*FA6a-GFP(S65T)::natMX6*	Euroscarf (Van Driessche et al., 2005)
YCplac33-p*MET3::URA3*	This study
YCplac33-p*MET3-eCFP-TUB3::URA3*	This study

Table S5: Yeast strains used.

Strain number	Genotype	Source
JVG1367	MAT**a** *his3Δ1 leu2Δ met15Δ ura3Δ*	Euroscarf
JVG1368	MATα *his3Δ1 leu2Δ lys2Δ ura3Δ*	Euroscarf
JVG1362	MATα *Mfa1Δ::MFA1pr-HIS3 can1Δ his3Δ leu2Δ ura3Δ MET15*$^{+}$ *lys2Δ*	C. Boone (Tong et al., 2001)
JVG4462	as JVG1368 *ade2::kanMX*	Euroscarf
JVG1371	as JVG1367 *rom2::kanMX*	Euroscarf
JVG3711	as JVG1362 *rom2::natMX*	this study
JVG1482	as JVG1367 *tus1::kanMX*	Euroscarf
JVG3713	as JVG1362 *tus1::natMX*	this study
JVG1552	as JVG1367 *rom1::kanMX*	Euroscarf
JVG4575	*rom2::natMX rom1::kanMX +pROM2*	this study
JVG3654	*rom2::natMX tus1::kanMX*	Krause et al., 2008
JVG3659	*rom2::natMX tus1::kanMX*	Krause et al., 2008
JVG3990	*rom1::kanMX tus1::natMX*	this study
JVG4531	*ade2::kanMX rom2::kanMX*	this study
JVG4538	*ade2::kanMX tus1::kanMX*	this study
JVG3340	*ack1::kanMX rom2::natMX lrg1::LEU2*	this study
JVG3339	*rom2::natMX rom1::kanMX lrg1::LEU2*	this study
JVG4729	*TUS1-13MYC::HIS*	D. Pellman(Yoshida et al., 2006)
JVG4762	*ack1::natMX TUS1-13MYC::HIS*	this study
JVG4799	*rgl1::natMX TUS1-13MYC::HIS*	this study
JVG1886	as JVG1367 *ack1::kanMX*	Euroscarf
JVG3713	as JVG1362 *ack1::natMX*	this study
JVG1941	as JVG1367 *ypl066w::kanMX*	this study
JVG3888	*ack1::natMX rom1::kanMX*	this study
JVG2979	*ack1::natMX tus1::kanMX*	this study
JVG3372	*ack1::natMX ypl066w::kanMX*	this study
JVG3384	*rom2::natMX ypl066w::kanMX*	this study
JVG3393	*tus1::natMX ypl066w::kanMX*	this study
JVG1367	MATa *his3Δ1 leu2Δ met15Δ ura3Δ*	Euroscarf
SSC2711	MATa *his3Δ1, ura3Δ0, leu2Δ0, lys2Δ0 ack1::kanMX4 TUS1-GFP::natMX6* [YCplac33-p*MET3-eCFP-TUB3::URA3*]	this study
SSC2712	MATa *his3Δ1, ura3Δ0, leu2Δ0 ypl066w::kanMX4 TUS1-GFP::natMX6* [YCplac33-p*MET3-eCFP-TUB3::URA3*]	this study
SSC2714	MATa *his3Δ1, ura3Δ0, leu2Δ0, lys2Δ0 ack1::kanMX4 ROM2-GFP::natMX6* [YCplac33-p*MET3-eCFP-TUB3::URA3*]	this study
SSC2715	MATa *his3Δ1, ura3Δ0, leu2Δ0 ypl066w::kanMX4 ROM2-GFP::natMX6* [YCplac33-p*MET3-eCFP-TUB3::URA3*]	this study
SSC2763	MATa *his3Δ1, ura3Δ0, leu2Δ0 TUS1-GFP::natMX6* [YCplac33-p*MET3::URA3*]	this study

SSC2766	MATa *his3Δ1, ura3Δ0, leu2Δ0 ROM2-GFP::natMX6* [YCplac33-p*MET3::URA3*]	this study

A.

	Benomyl	Chloropromazine
Wild type	+	+
rom2	-	+
rom2 + p*TUS1*	+	+
tus1	+	-
tus1 + p*ROM2*	+	+

B.

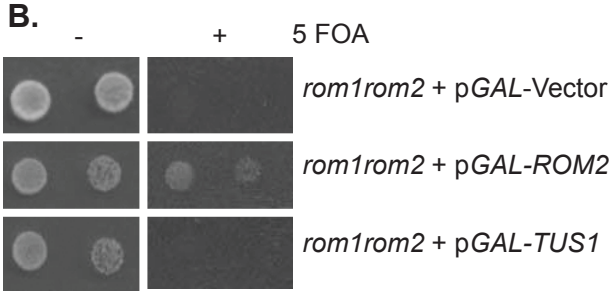

Sup. Figure1

A.

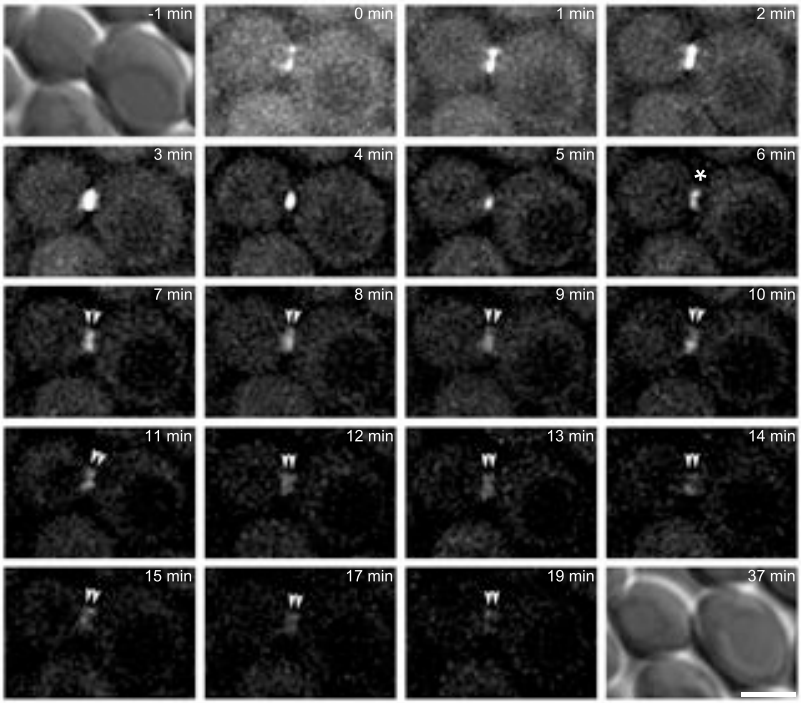
-1 min
0 min
1 min
2 min
3 min
4 min
5 min
6 min
*
7 min
8 min
9 min
10 min
11 min
12 min
13 min
14 min
15 min
17 min
19 min
37 min

B. **C.**

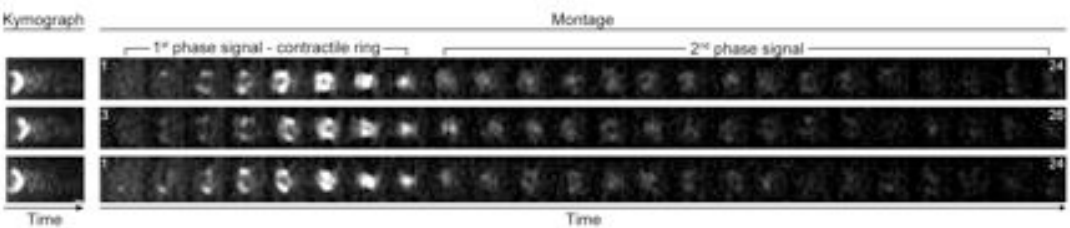
Kymograph
Montage
1st phase signal - contractile ring
2nd phase signal
Time
Time

A.

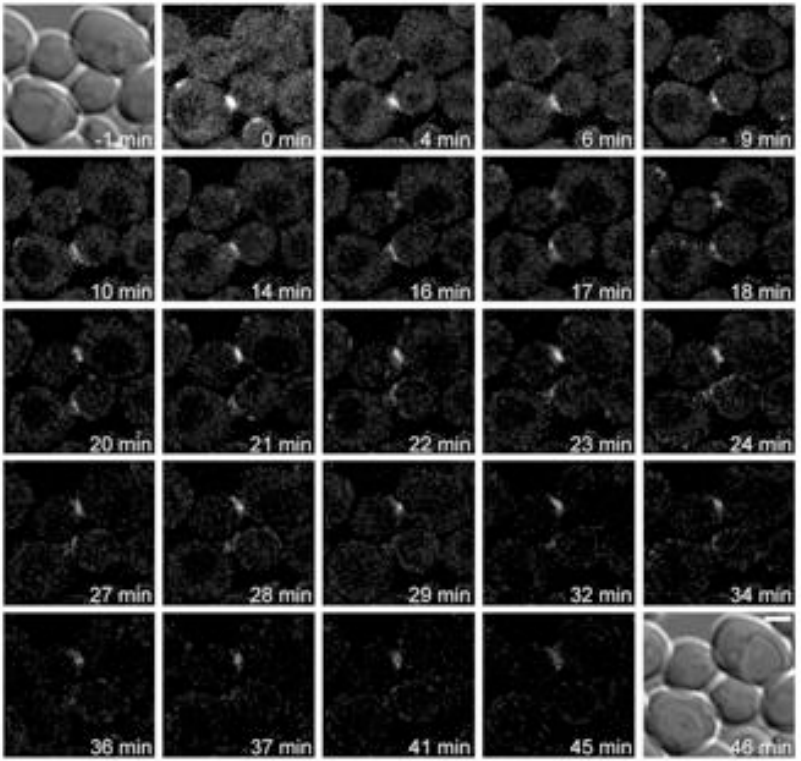
-1 min
0 min
4 min
6 min
9 min
10 min
14 min
16 min
17 min
18 min
20 min
21 min
22 min
23 min
24 min
27 min
28 min
29 min
32 min
34 min
36 min
37 min
41 min
45 min
46 min

B. **C.**

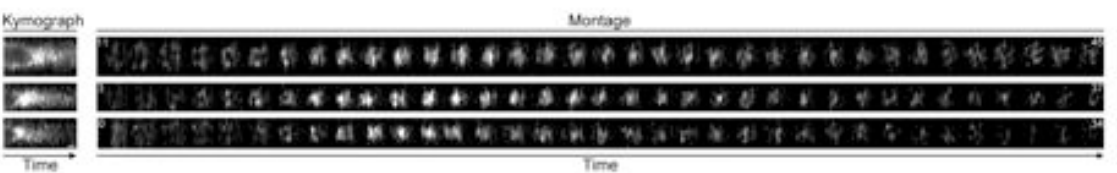
Kymograph
Montage
Time
Time

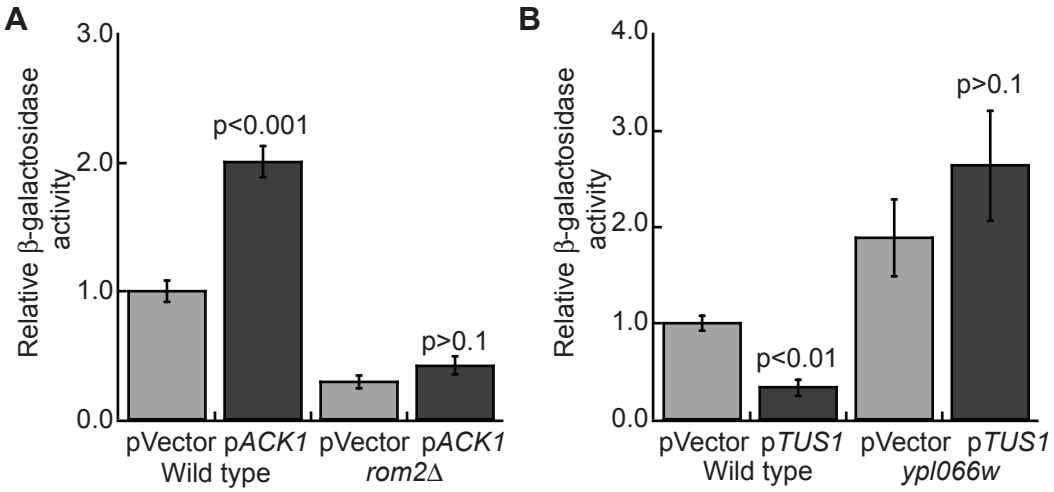
A
Relative β-galactosidase activity
3.0
2.0
1.0
0.0
p<0.001
p>0.1
pVector
pACK1
pVector
pACK1
Wild type
rom2Δ
B
Relative β-galactosidase activity
4.0
3.0
2.0
1.0
0.0
p>0.1
p<0.01
pVector
pTUS1
pVector
pTUS1
Wild type
ypl066w

Sup Figure 4

A. *TUS1-GFP ack1Δ*

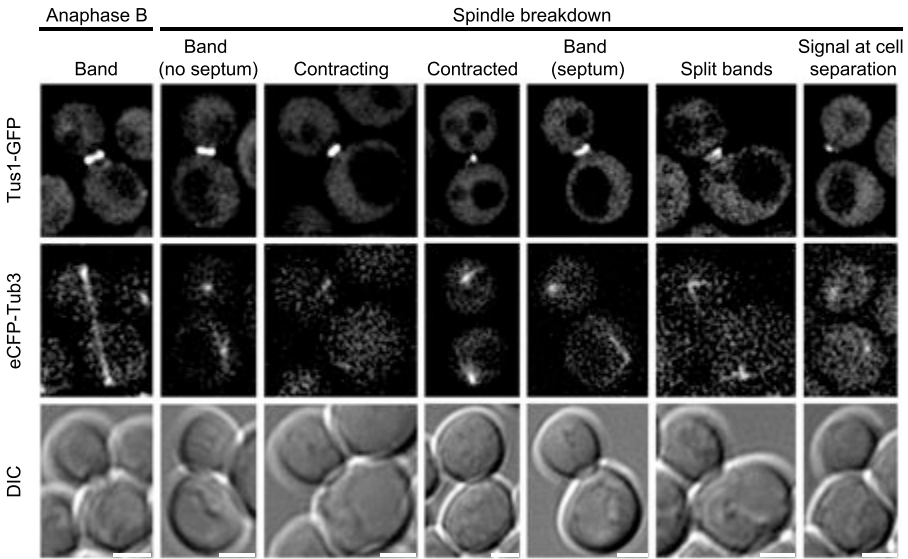

A. *ROM2-GFP ypl066wΔ*

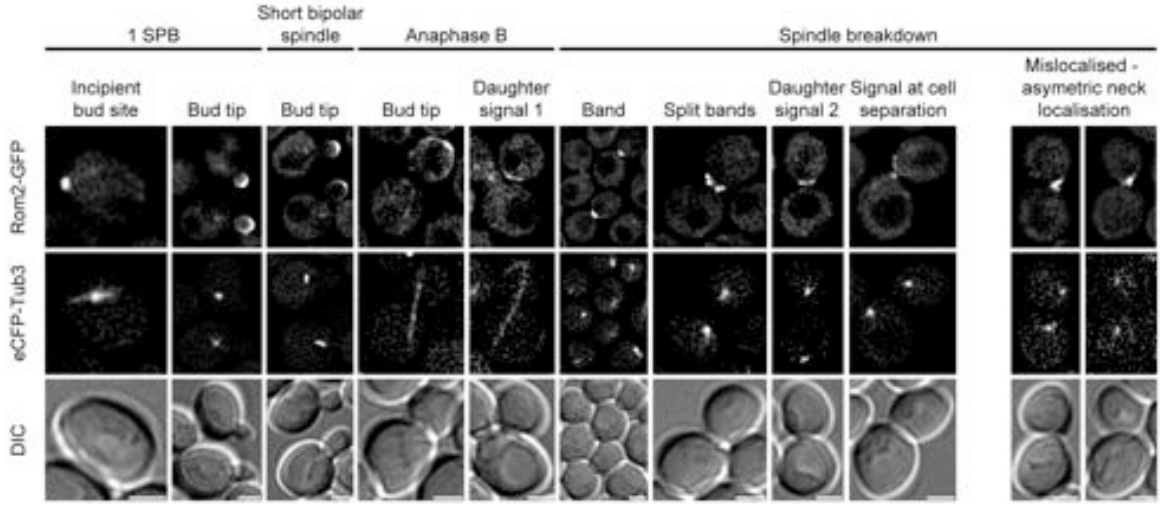

B.

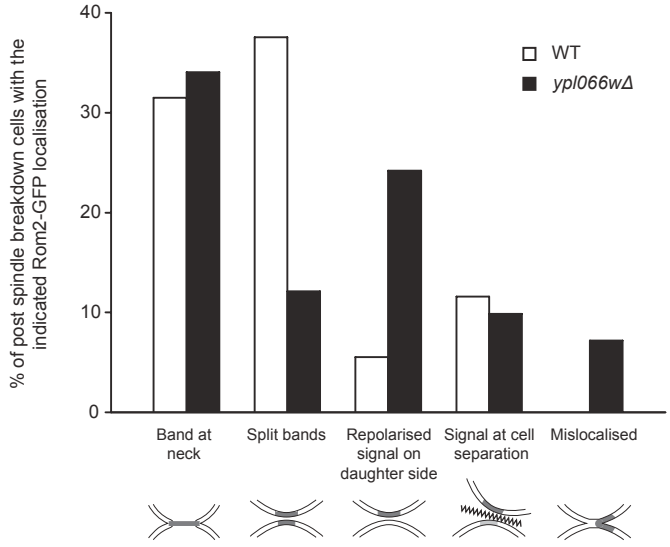

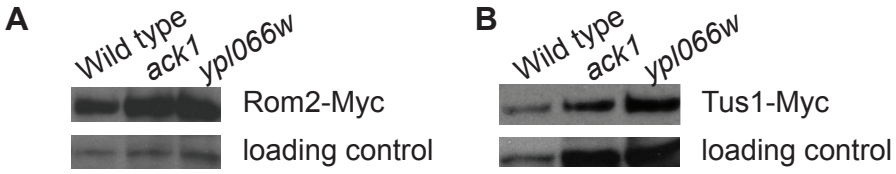
A
Wild type
ack1
ypl066w
Rom2-Myc
loading control
B
Wild type
ack1
ypl066w
Tus1-Myc
loading control

Sup Fig 7